DOE/ET/15365--T2

stonehart associates

DOE/ET/15365--T2

DE82 006984

PREPARATION AND EVALUATION OF ELECTROCATALYSTS FOR PHOSPHORIC-ACID FUEL CELLS

Final Technical Report
May 1, 1978 - December 31, 1979

Contract No. DE-AC03-78ET15365

Prepared for: Department of Energy (Attn: G. Hagey)
Office of Coal Utilization
Washington, D.C. 20545

Program Manager: P. Stonehart
J. Baris, Senior Scientist

MASTER

Technical Manager: NASA-Lewis Research Center
Milton R. Lauver
Fuel Cell Project Office

17 Cottage Road, Madison, Connecticut 06443
Telephone Area Code 203 245-7507

DISCLAIMER

NOTICE

This report was prepared as an account of work sponsored by an agency of the United States Government. Neither the United States nor any agency thereof, nor any of their employees, nor any of the contractors, subcontractors, or their employees, makes any warranty, expressed or implied, or assumes any legal liability or responsibility for any third party's use or the results of such use of any information, apparatus, product or process disclosed in this report or represents that its use by such third party would not infringe privately owned rights.

stonehart associates

TABLE OF CONTENTS

17 Cottage Road, Madison, Connecticut 06443

Telephone Area Code 203 245-7507

ABSTRACT

The overall objective of this electrocatalysis program was to define the feasibility of lowering the electrocatalyst cost and to increase the electrocatalyst activity in phosphoric acid fuel cells to improve the commercial viability of fuel cells for producing electric power.

Highly dispersed platinum was placed on carbon supports that were developed under the EPRI RP 1200-2 program so that they could be used as phosphoric acid fuel cell electrocatalysts. These catalysts were characterized for both the platinum surface areas and crystallite sizes. For a given carbon impregnation technique with the noble metal salt, a definite correlation between the specific surface area of the derived platinum crystallites and the BET surface area of the carbon support was found. A high dispersion of platinum was achieved on a novel high surface area catalyst support - CONSEL.

Using high resolution phase contrast electron microscopy, the crystal lattice of highly dispersed platinum on carbon was resolved and, with the lattice images of graphitic carbon black as an internal calibration, the lattice spacing for a small crystallite of platinum was measured within 2% of the value for bulk platinum.

Twenty-one catalysts were formulated with variations in the type of carbon support, the platinum metal loading, and the platinum crystallite size. A half-cell apparatus was constructed to determine the catalytic activity of high surface area platinum on carbon electrocatalysts for the electrochemical reduction of oxygen in concentrated phosphoric acid at elevated temperatures. Teflon-bonded, gas-diffusion electrodes were fabricated on porous carbon substrates and were tested in a floating mode using 102 w/o phosphoric acid at 180°C. The iR-free electrode potentials were measured relative to a reversible hydrogen reference and were plotted against the log-current to obtain activity and Tafel slope information as diagnostics. In addition, gas-diffusion electrodes were formed from selected electrocatalysts and their performances evaluated for oxygen reduction and hydrogen oxidation in 100 w/o phosphoric acid at 180°C. The iR-free potentials were measured as a function of the current densities and the specific reaction rates were computed as a function of the platinum crystallite sizes.

For oxygen reduction, analysis of the polarization curves suggests that improvement in electrode structures is required since diffusion controlled operation was evident even at low current densities. For hydrogen oxidation, efficient electrodes were fabricated for the oxidation of hydrogen molecules. The degree of poisoning of the surface by carbon monoxide as a function of temperature was also obtained.

1. INTRODUCTION

The driving forces towards commercialization of fuel cell systems are efficient utilization of the fuel, low pollution (including noise as a pollutant) and the fact that fuel cell power plants do not incur a penalty of lower efficiency when they operate at power levels less than the design maximum. The concept of electric power generation by fuel cells needs no introduction. With hydrocarbon fuels, gas phase fuel treatments are used to produce hydrogen which is oxidized electrochemically. Carbon dioxide is present in the fuel gas stream so alkaline electrolytes are precluded from low temperature fuel cell consideration. Emphasis has, therefore, been placed on phosphoric acid systems.

Cost is a critical factor in the application of phosphoric acid fuel cell systems for producing electrical power. In turn, efficiency of the electrocatalysts must be high for fuel cell systems to become commercially viable. Present phosphoric acid fuel cells use platinum as the catalyst on both the anode and cathode. As a result of considerable research in the last ten years, the combined platinum loading of the anode and cathode is now less than 1 mg/cm^2. This has been accomplished by supporting platinum on high surface area, conductive carbon blacks. The resulting platinum crystallites are small, i.e. on the order of 30 $\mathring{A}$.

It can be reasoned that, since there are so few atoms in small crystallites, the metallurgical and chemical properties of the bulk material do not hold when very small particles are obtained. Recently, it has been claimed that the catalytic activity of platinum decreases as the surface area of the catalyst is increased (1). Even if this is so, small crystallites are more efficient in the current density range of practical interest, because a decrease in Tafel slope is associated with increased catalyst surface area.

The preparation of high surface area electrocatalysts is, therefore, an important aspect of fuel cell technology. Highly dispersed electrocatalytic

materials have been reviewed by Kinoshita and Stonehart (2). They discussed details of various catalyst preparation techniques. Among these, impregnation of metal salt on a suitable inert support has been widely accepted as an industrial process.

The overall objective of this electrocatalysis program was to define the feasibility of lowering the electrocatalyst cost and to increase the electrocatalyst activity in phosphoric acid fuel cells to improve the commercial viability of fuel cells for producing electric power. The specific objectives were to prepare a series of high surface area electrocatalysts, to utilize these electrocatalysts in the fabrication of efficient gas-diffusion electrode structures, and to determine their electrochemical parameters for oxygen reduction and hydrogen oxidation. In addition, the degree of poisoning by carbon monoxide at the hydrogen electrode was to be investigated.

2. CATALYST PREPARATION AND CHARACTERIZATION

Support Selection

A number of carbons have been identified and characterized by Stonehart Associates, Inc. under the EPRI RP 1200-2 program. From these, the following carbons were selected to represent a cross section of presently viable electrocatalyst supports:

Vulcan XC-72R	as received
Vulcan XC-72R	1200HT
Vulcan XC-72R	1400HT
Vulcan XC-72R	1800HT
Vulcan XC-72R	2500HT
Vulcan XC-72R	2700HT
Vulcan XC-72R	3000HT
AC BL	as received
AC BL	1200HT
AC BL	2500HT
*CONSEL	as received

* Steam treated AC BL

In order to carry out the research to determine whether the structure of the carbon support was influencing the reactivity of the platinum crystallites for oxygen reduction, it was necessary to prepare a series of catalysts with well-characterized carbon structures and platinum dispersions.

Preparation

Typically, 10 w/o platinum on carbon electrocatalysts were prepared from chloroplatinic acid by the following procedure. Carbon black samples (1 to 2 g) were wetted by pouring the appropriate amount of aqueous solution of H_2PtCl_6 (10 mg Pt/ml of solution) onto the powder. After a brief ultrasonic agitation the solution was completely impregnated into the porous carbon black and no free solution was observed. The mixture was air dried in an oven at about 60°C. This dried catalyst was ground in a mortar and placed in a tube furnace. After purging with helium for about 2 hours, pure hydrogen was introduced and the temperature increased rapidly to 200°C. The hydrogen reduction was carried out for 1 hour. The reduced or "activated" catalyst was then cooled to room temperature in helium. In addition, several catalysts were prepared having platinum loadings of 1, 5, 15, and 20 w/o. The series of electrocatalysts is given in Table 1 together with the platinum metal loading, platinum surface area and the carbon support BET surface area. These catalysts were characterized by slug flow CO chemisorption and electrochemical hydrogen adsorption to obtain the specific surface area of platinum. Some of these catalysts were also examined by ultra-high resolution transmission electron microscopy, thin section transmission electron microscopy, and/or x-ray diffraction.

Chemisorption Characterization

In the slug flow CO chemisorption method (3), a stream of helium was passed over the reduced or "activated" catalyst sample and a known amount of CO injected into the helium stream. The amount of CO not adsorbed and therefore remaining in the helium stream was measured by a thermal conductivity bridge detector. The amount of CO adsorbed on the Pt surface was obtained by the difference of this response and the response of the slug obtained in a blank run. The adsorbed CO per gram of catalyst is a measure of metal dispersion and is directly converted to specific surface area of the platinum crystallites by means of the following equation:

$$S = 0.811 \left(\frac{P}{T}\right) \left(\frac{V}{W}\right) \qquad \text{Equation (1)}$$

where S = Pt surface area, m^2/g; P = ambient pressure, Torricelli; T = ambient temperature, °K; V = volume CO adsorbed, cc NTP; and W = weight Pt in catalyst sample, g.

Table 1: Electrocatalyst Series

DOE Number	Weight Percent Platinum	Platinum Surface Area in m^2/gm CO	Platinum Surface Area in m^2/gm ECA	Carbon	Carbon Surface Area m^2/gm BET
1	10	153	133	*XC-72R	250
2	10	137		XC-72R	250
3	10	154		XC-72R 1200 HT	174
4	10			XC-72R 1400 HT	140
5	10			XC-72R 1800 HT	95
6	10	62	65	XC-72R 2500 HT	65
7	10			XC-72R 2700 HT	63
8	1	48		XC-72R 3000 HT	60
9	10	81		XC-72R 3000 HT	60
10	10		86	AC BL	65
11	10	92		AC BL 1200 HT	62
12	10	58	61	AC BL 2500 HT	44
13	20	60	68	AC BL	65
14	15	64		AC BL	65
15	10	72	80	AC BL	65
16	5	92	93	AC BL	65
17	1	128	140	AC BL	65
18	10		80	AC BL 400 HT	
19	10		82	AC BL 600 HT	
20	10		80	AC BL 800 HT	
21	10		56	AC BL 950 HT	

* Vulcan XC-72R as received.

The area of surface platinum atoms has been taken as 8.4 $\mathring{A}$ (4).

Surface area measurements were also made using an electrochemical technique (5,6). Porous flooded structure electrodes with small amounts of PTFE were prepared on a porous carbon substrate. These electrodes were placed in a Model 494 Universal Cell and a periodic triangular potential sweep was applied to the BC 1200 potentiostat. The electrolyte was 50 w/o H_3PO_4 saturated with nitrogen. Platinum catalyst surface areas were determined from the total coulombic charge required for hydrogen adsorption, after correcting for double layer charging, using 210μC/real cm^2 Pt. This corresponds to 1.305×10^{15} atoms/cm^2 and assumes each surface platinum atom adsorbs one hydrogen atom. A typical voltammetric sweep for a supported catalyst (10 w/o Pt on Vulcan XC-72R) in the flooded structure with 0.25 mg Pt per cm^2 of electrode is shown in Figure 1. The characteristics of the hydrogen on platinum voltammogram are described in detail elsewhere (4). The lack of resolution for the hydrogen peaks is characteristic of high surface area platinum (7). For this catalyst, the specific surface area of platinum was calculated to be 124 m^2/g while the CO adsorption gave 137 m^2/g of platinum.

Microscopic Characterization

Electron microscopy has been extensively used to characterize supported catalysts. Early work was limited to particle size determination and observation of spatial distribution of metal particles on the support material. Recently, high resolution electron microscopy by Prestridge, et al. demonstrated structural differences of small particles of ruthenium supported on alumina (8). Based on the differences in the optical density they concluded that some of the smaller particles were two-dimensional and raft-like. Ultra-high resolution electron microscopy has been used to study the microstructure and morphology of carbon blacks (9), and to obtain lattice images of Pt (111) planes using evaporated platinum films (10). More recently, with the new generation of microscopes, resolving power of 1.4 $\mathring{A}$ has been demonstrated by showing the lattice image of (220) planes in gold single crystals (11). Little, if any, of this technology has been applied towards characterization and understanding of highly dispersed electrocatalysts. It has been suggested that the very small platinum crystallites are amorphous or liquid-like and it has been argued that the non-crystallinity of small platinum particles may be a reason why the oxygen reduction characteristics of high surface area platinum are different from those of bulk platinum. There was no direct

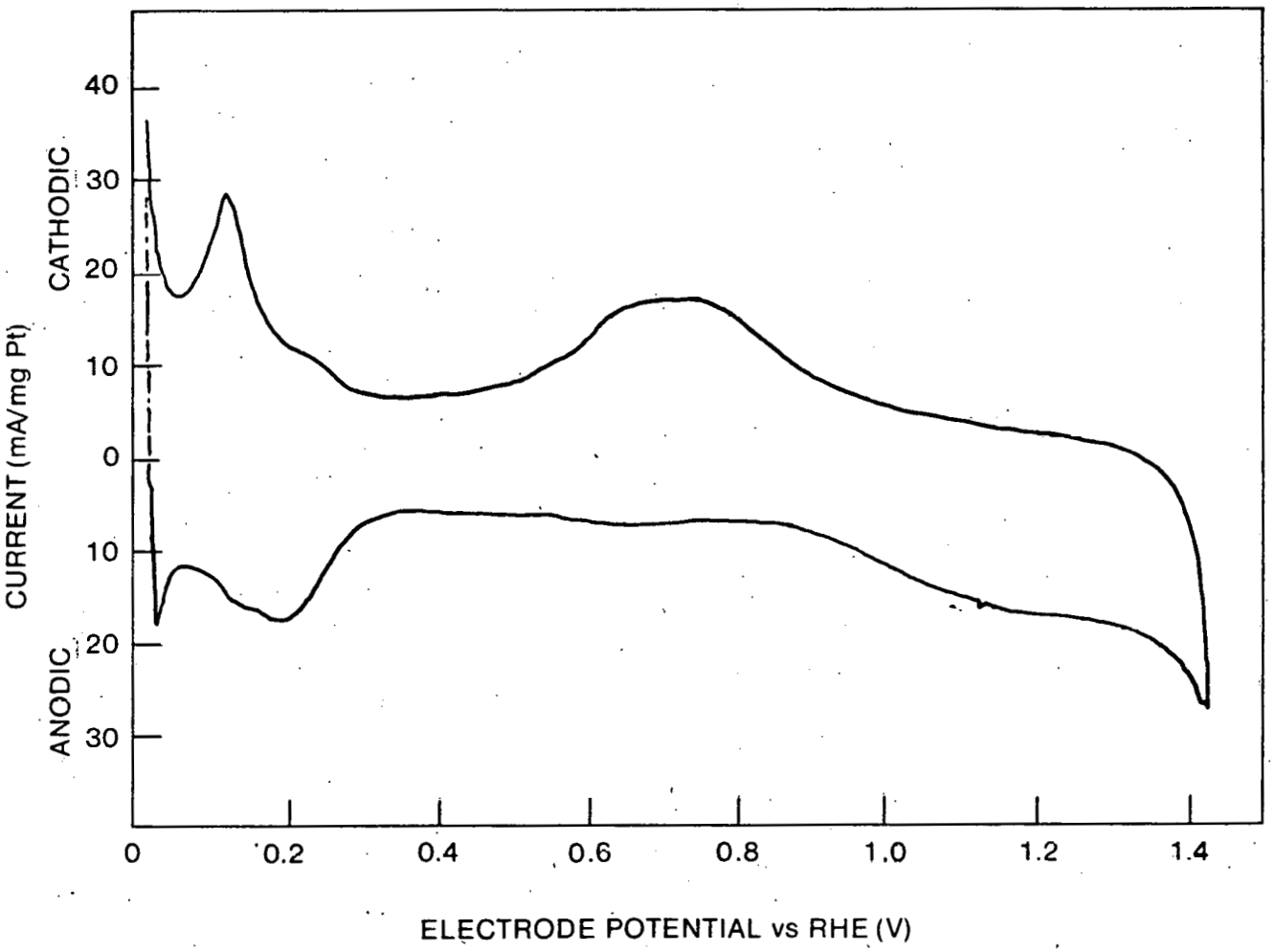

Figure 1. Potentiodynamic current/potential profile for 10 w/o Pt on Vulcan XC-72R in 50 w/o H_3PO_4 at 23°C; Sweeprate=.010 V/s.

evidence, however, that showed crystallinity or lack of it for very small platinum particles supported on carbon black. Due to the advent of ultra-high resolution electron microscopy, the microstructure of these very small platinum particles now has been viewed in a completely new way.

Using high resolution (lattice image) phase contrast microscopy, the crystal lattice of highly dispersed platinum supported on carbon black was resolved. This was achieved by the interference of the (111) diffracted beam with the central electron beam. A micrograph of 10% platinum on graphitized Vulcan is shown in Figure 2. These images show that fine particles of platinum down to 20 Å in diameter are crystalline in nature as opposed to amorphous or liquid-like.

The fringe images produced by phase contrast electron microscopy of fine platinum particles provide a novel tool to obtain structural information which could not have been deduced from x-ray diffraction studies.

Lattice dimensions of these small platinum crystallites were accurately measured. It has been established that the (002) spacing of graphitized carbon black is 3.44 Å (12). Extensive graphitic (002) layers and platinum (111) lattice layers are evident in the photographic print of Figure 2. The graphitic (002) lattice image was, therefore, used as an internal calibration to measure the (111) lattice spacing of platinum. A value of 2.30 Å was obtained; this value is within 2% of 2.27 Å, the (111) lattice spacing of bulk platinum.

A representative high resolution print of platinum on as-received Vulcan XC-72R is shown in Figure 3. This catalyst and the catalyst depicted in Figure 2 represents the two extremes in surface properties available with this support. These prints were used to substantiate the electrochemical surface area measurements for these two catalysts. Mean particle sizes of platinum crystallites were measured. Assuming a spherical geometry, the following equation was used to calculate the specific surface area S in m^2/g of platinum:

$$S = \frac{6}{pd} \times 10^4 \qquad \text{Equation (2)}$$

where d is the mean particle diameter in Å, and p is the density of platinum ($21.4\ g/cm^3$). This relationship is shown in Figure 4. In addition to confirming the surface area measurements by other methods, this technique reveals

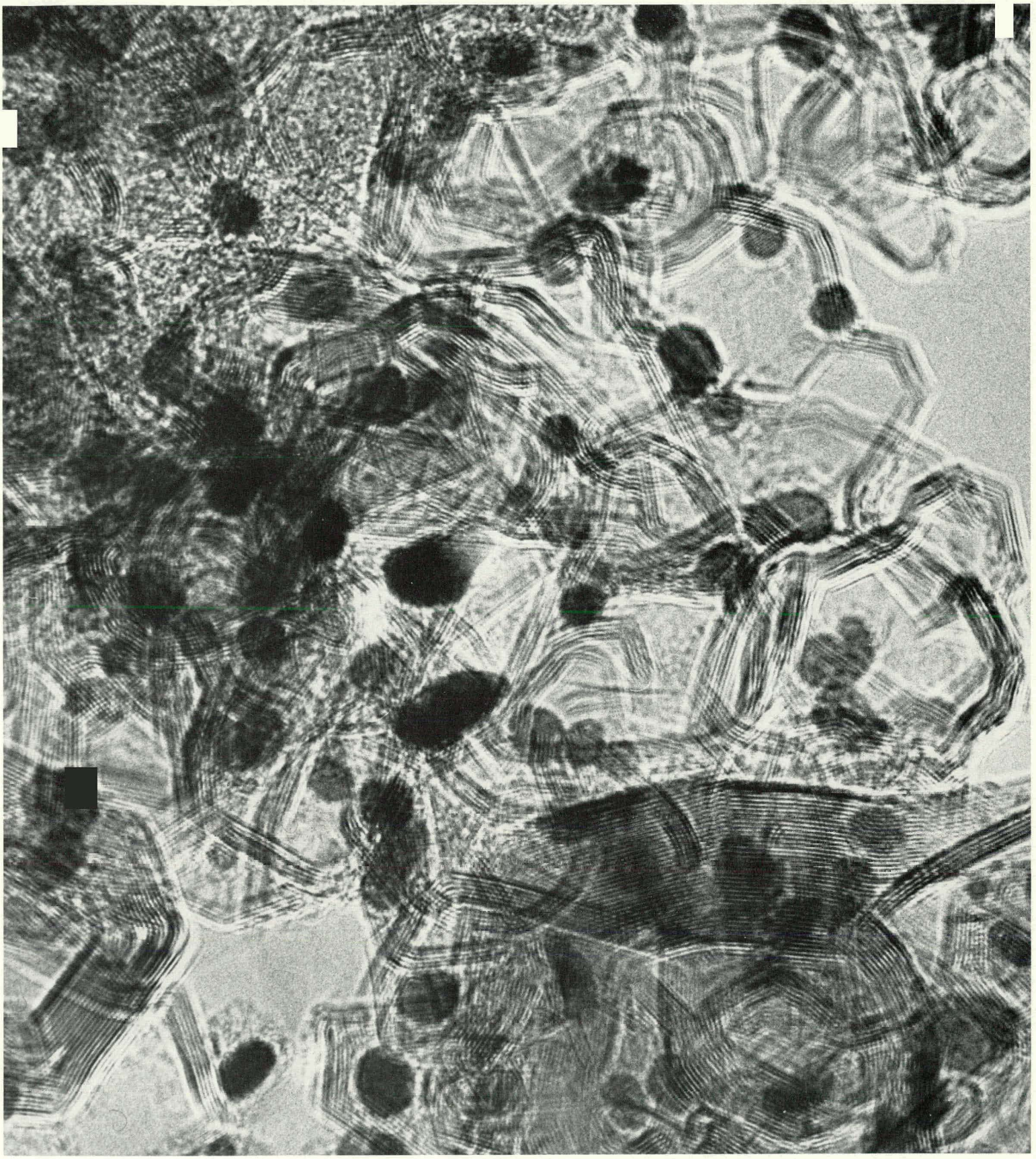

Figure 2. Phase contrast electron micrograph of 10 w/o Pt on graphitized Vulcan XC-72R. Magnification X 2,700,000; 1 mm = 3.7 Å.

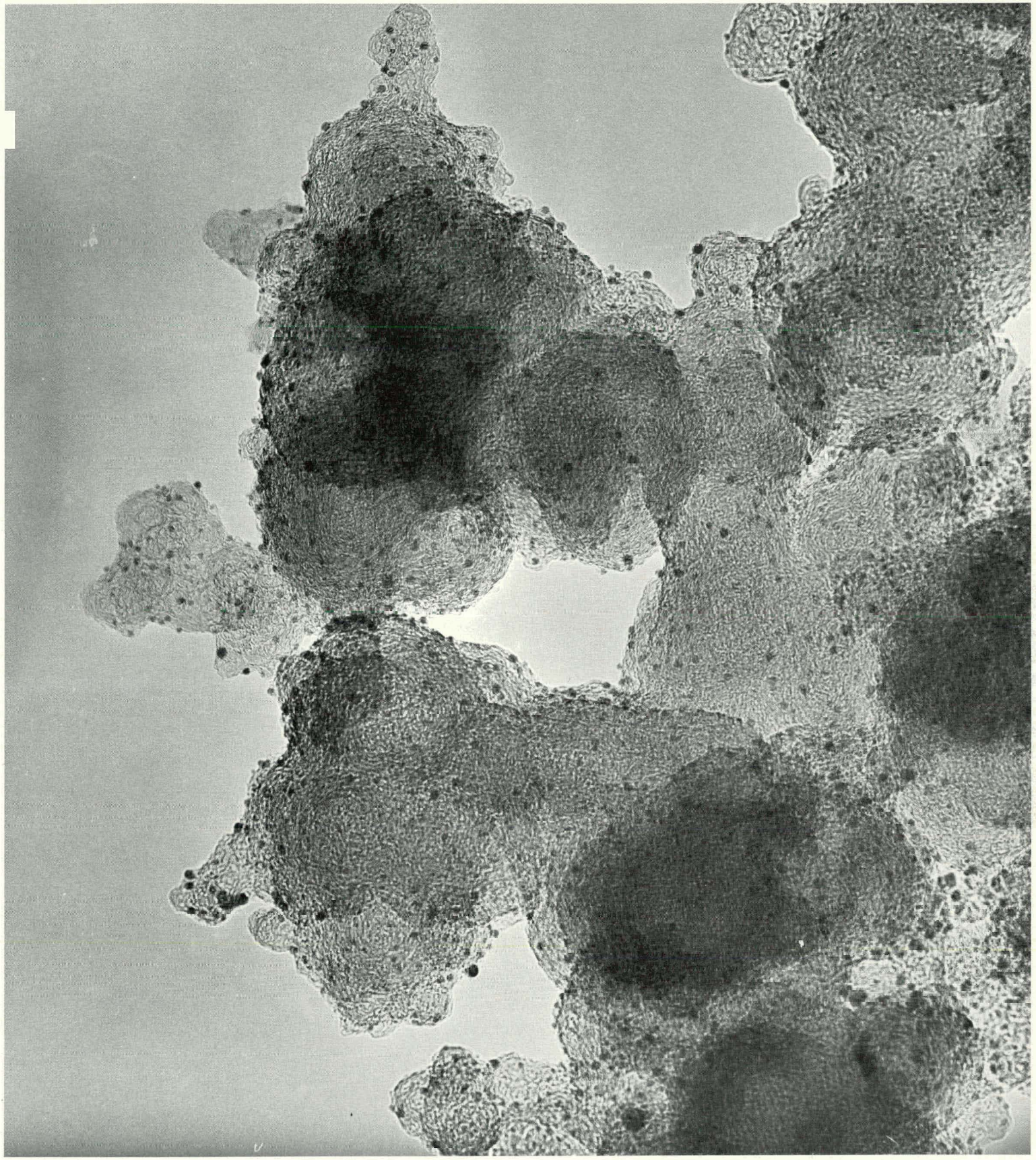

Figure 3. Electron micrograph of 10 w/o platinum supported on Vulcan XC-72R. Magnification X 830,000; 1 mm = 12 Å.

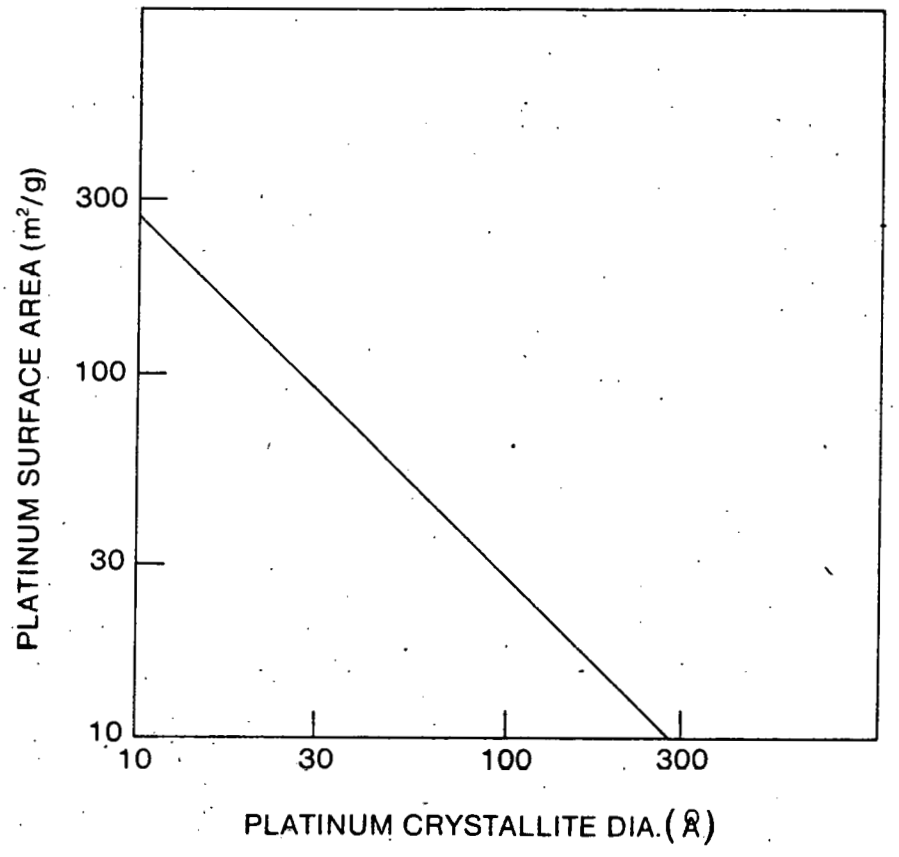

Figure 4: The relationship between the platinum crystallite size and the specific surface area according to Eqn. (2).

the particle size distribution, the spatial dispersion, and the morphology of the support material. From the catalyst samples examined, the particle size distribution appeared to be uniform.

Ultramicrotomy for TEM is commonly used in biological sciences. However, ultramicrotomy of hard inorganic materials such as carbon supported catalysts require high levels of technical skill. This technique involves:

- Embedding in a suitable medium which could vary from catalyst to catalyst depending on the final cure hardness properties of the resin used.
- Thin sectioning with a carefully selected diamond knife. The cutting speed and the angle of the knife are critical factors in obtaining thin sections and are dependent on the choice of the embedding resin and the type of diamond knife.

With this aim, three samples of platinum on carbon catalysts were analyzed by Structure Probe, Inc., which has the capability for diamond knife thin-sectioning of hard inorganic materials. The quality of the sections as reflected in the transmission electron micrographs were not suitable for obtaining the desired information. It appeared that the embedding medium did not form a bond with the carbon particles and hence instead of forming a slice, the carbon particles were peeled off the resin. It was also evident that during the process of sample preparation, the platinum particles were dislodged from the catalyst support. The fuel cell catalysts developed in this work have very small platinum particle size (about 10 - 25 $\mathring{A}$) and are supported on high surface area carbon blacks. For such work the presence of an embedding resin causes loss of resolution.

In summary, although some general information on the platinum particle size and gross differences in the carbon supports can be observed, the thin-sectioning method not only showed no advantages over conventional electron microscopy of such catalysts, but also destroyed the spatial distribution of the supported metal particles and produced inferior resolution. The embedding and ultramicrotomy techniques need to be developed further for a meaningful thin-sectioning of such materials.

X-Ray Characterization

In addition to CO adsorption, electrochemical hydrogen deposition and electron microscopy, x-ray line broadening was used to characterize two of the electro-

catalysts - 10 w/o Pt on as-received Vulcan XC-72R and 10 w/o Pt on graphitized (3000HT) Vulcan XC-72R. For highly dispersed platinum crystallites, the x-ray peaks are diffuse and broad. Further complications arise due to interference from the support material. The measured half widths were corrected for the instrument line width. Average platinum crystallite sizes were calculated using the Scherrer equation. Assuming a spherical geometry, the specific surface area of platinum was calculated by Eqn. (2).

Characterization Summary

Table 2 summarizes platinum crystallite size and the corresponding specific surface areas using different measuring techniques. Considering the difficulties involved for measuring very high surface areas, the agreement among various techniques for the 10 w/o Pt on Vulcan XC-72R is quite reasonable and for 10 w/o Pt on graphitized carbon support is exceptionally good.

Analytical data for selected carbons and electrocatalysts containing 10 w/o platinum are presented in Table 3. The heat-treated carbons have improved corrosion resistance from the point of view of carbon loss under operating fuel cell conditions. It should be noted, however, that the heat treatment also reduces the support surface area. During the course of this work it was found that for the impregnation catalyzation process, the specific surface area of platinum crystallites deposited on carbon was related to the BET surface area of the support. Figure 5 demonstrates that higher platinum surface areas can be realized on supports exhibiting higher BET surface areas. A similar relationship between platinum crystallite surface area and BET area has been reported previously (13). In this study, carbon supports with large differences in crystal structure (amorphous to graphitic) and surface properties (as measured by volatile contents and pH) were selected for catalyzation. The data are shown in Figure 6. Note that the scale in Figure 6 is different from that used in Figure 5. Although there is some scatter, a definite increase of platinum surface area with increased surface area of carbon support can be seen. Part of the scatter is believed to be due to inadequacy of the N_2 adsorption BET method to distinguish between true and available surface areas for microporous materials (14).

The crystallite surface area versus BET surface area correlation can be explained by a number of theories; the simplest of them being that carbon defects act as trap sites for platinum crystallites. Graphitic carbons have

Table 2: Platinum Crystallite Size Comparison Using Different Measuring Techniques

Catalyst	CO Adsorption		Electrochemical		Electron Microscopy		X-ray Diffraction	
	S m^2/g	d_o Å	S m^2/g	d_o Å	S m^2/g	d_o Å	S m^2/g	d_o Å
10 w/o Pt on Vulcan XC-72R	137	20*	124	23*	165*	17	156*	18
10 w/o Pt on Graphitized XC-72R	81	35*	81	35*	76*	37	80*	35

* The average particle sizes were calculated from Pt surface area assuming spherical particles and using Equation (2) and vice versa.

Table 3: Properties of Selected Carbons and Electrocatalysts

Carbon	Heat Treatment Temperature ^{o}C	BET Surface Area m^2/g	Specific Carbon Corr. Rate at 1000 min, 0.7 V, 210^{o}C $mA/cm^2 \times 10^7$	Platinum Cryst. Surface Area m^2/g
Vulcan XC-72R	None	254	4.2	153
Vuclan XC-72R	None	254	4.2	171
Vulcan XC-72R	1200	174	1.5	154
Vulcan XC-72R	1400	140	-	107
Vulcan XC-72R	1800	95	-	81
Vulcan XC-72R	2500	65	.15	62
Vulcan XC-72R	2700	60	-	77
Vulcan XC-72R	3000	50	.095	81
Shawinigan Ac Blk.	None	65	.12	82
Shawinigan Ac Blk.	1200	62	.8	92
Shawinigan Ac Blk	2500	45	.25	58
CONSEL	-	247	.033	138

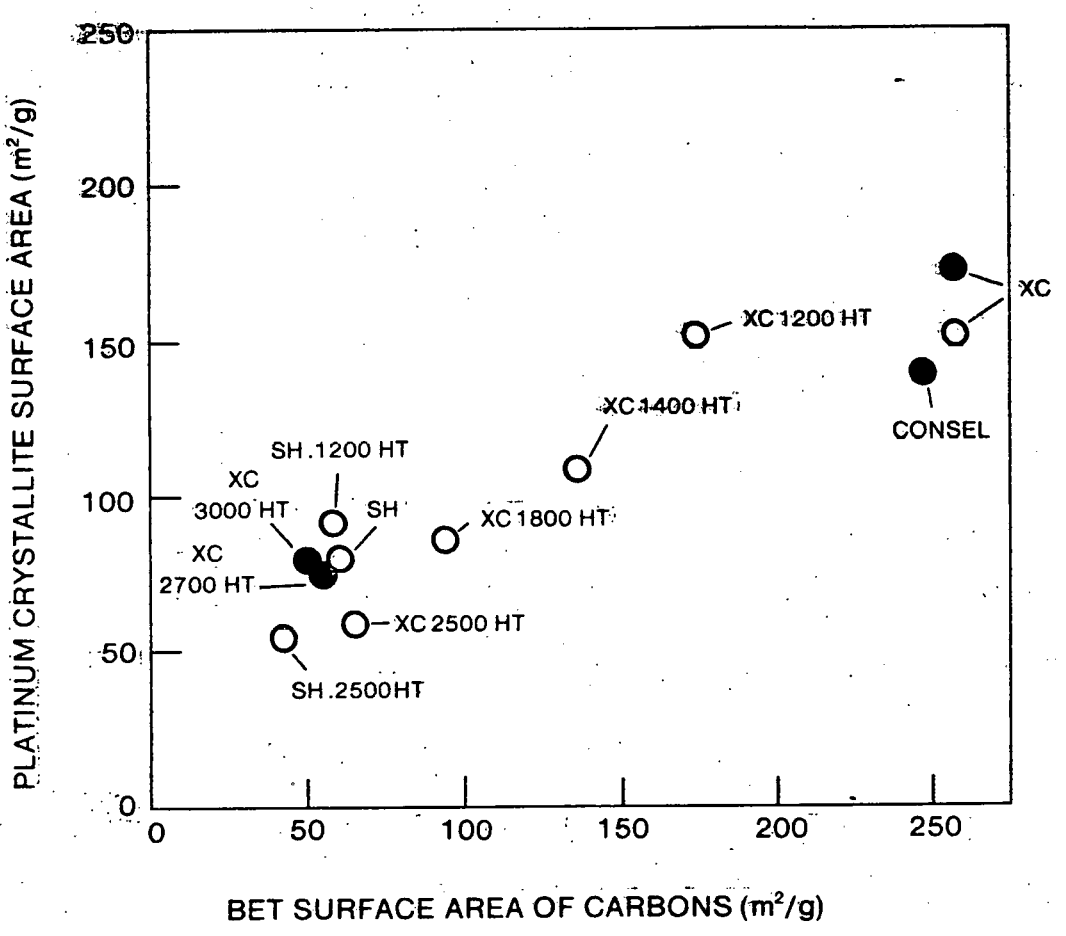

Figure 5. Platinum crystallite surface areas at 10 w/o Pt loading as a function of the carbon support surface areas.

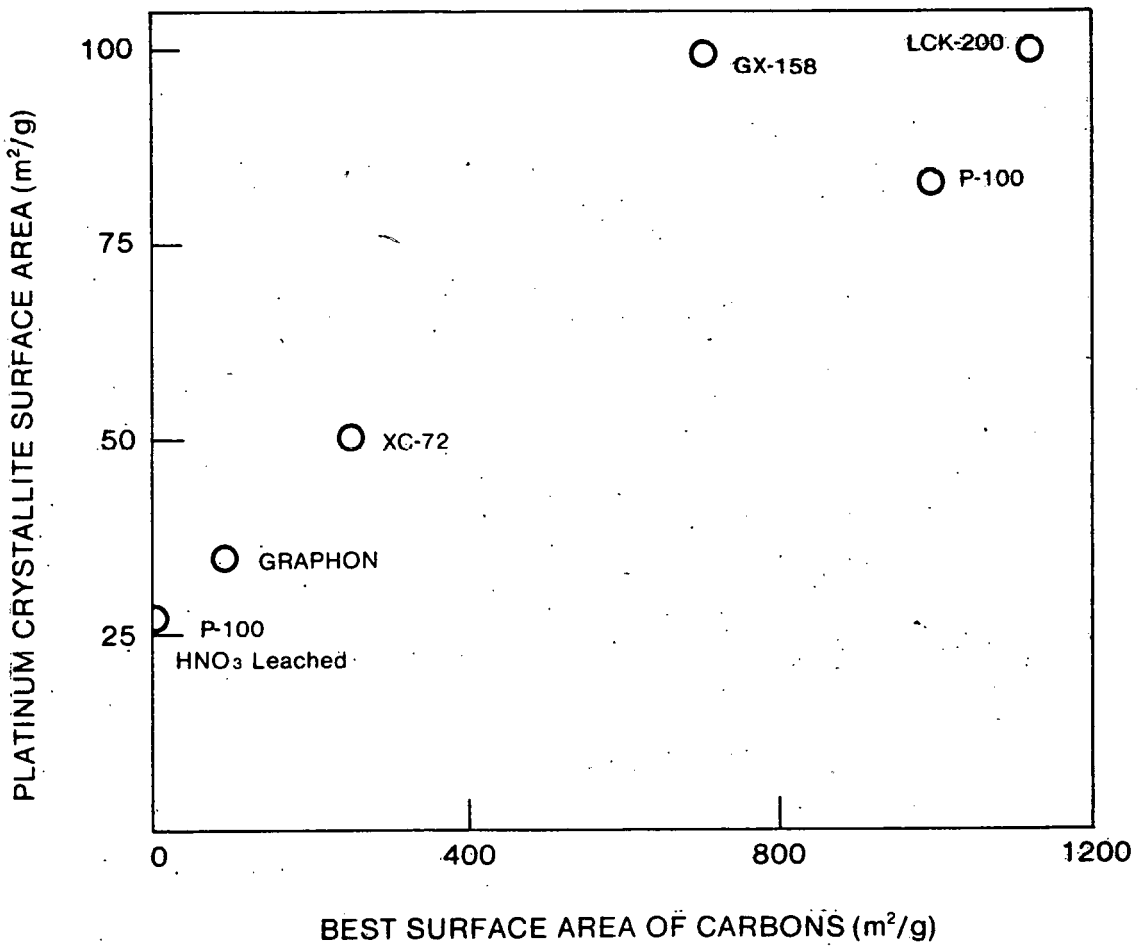

Figure 6. Platinum crystallite surface areas at 10 w/o Pt loading as a function of the carbon support surface areas.

lower surface areas, hence, fewer defect sites than turbostratic carbon blacks. Carbons with lower surface area should have relatively fewer defect sites. As a result, the platinum crystallites should be larger than those on high surface area carbons for a given platinum loading. Since the number of growth sites for Pt crystallites may be considered constant for a given carbon sample, the deposition of less Pt, e.g. 1% loading, should be expected to give smaller crystallites. As a test of this theory, electrocatalysts with only 1 w/o platinum were prepared on as-received Vulcan XC-72R (BET surface area 254 m^2/g) and Vulcan XC-72R 3000HT (BET surface area 60 m^2/g). The electron micrographs indicated that even for 1 w/o platinum loading, the size of the crystallites on graphitized carbon black were larger than those on the high surface area carbon black. For a given carbon support, platinum crystallite size was about the same for both 10 w/o Pt and 1 w/o Pt loadings. Some of the results in Table 1, however, show the expected differences based on CO and ECA measurements. Other related factors such as wettability and microporosity of the support material will influence the catalyzation.

There is still considerable room for catalyst improvement. The platinum surface area, for example, will approach 250 m^2/g if all atoms are surface atoms. This limiting surface area has not been approached in this work.

3. ELECTROCHEMICAL EVALUATION

Experimental

A half-cell apparatus was constructed to determine the catalytic activity of high surface area platinum supported on carbon for the electrochemical reduction of oxygen and oxidation of hydrogen in concentrated phosphoric acid at elevated temperatures. The performance measurements were made with this apparatus using PTFE-bonded gas-diffusion electrodes on porous carbon substrates. Prior to the catalyst layer deposition, the carbon substrate was wetproofed using a PTFE emulsion to provide the gas diffusion path. The catalyst was dispersed in water using ultrasonic agitation and TFE-30 dispersion was added to give a 50 w/o catalyst to PTFE content. The solution was filtered directly onto the carbon substrate. Following air drying at about 75°C, the electrode was placed in a sintering oven at 330°C for 15 minutes. Some electrodes were also prepared using Teflon-3416 emulsion. Since Teflon 3416 has a significantly lower surfactant concentration than Teflon-30, the rate of flocculation, hence, the agglomerate size, is more easily controlled. Electrodes were prepared using each of the catalysts listed in Table 1.

The floating mode method described by Giner and Smith (15) was used to test 1 cm^2 electrodes in 102 w/o H_3PO_4 at 180°C for oxygen reduction activity. The acid concentration was maintained by presaturating the reactant gas (O_2 or air) to provide a water vapor pressure in equilibrium with the electrolyte. Temperatures of both the test cell and presaturator were controlled to within ±1°C by proportional controllers. The electrode potentials were measured relative to a reversible hydrogen reference electrode in the same electrolyte. A BC-1200 potentiostat was used in both the potentiostatic and galvanostatic modes for these measurements. The electrode potentials were iR corrected.

iR correction and compensation for the resistive losses can be demonstrated by constancy of the corrected output during translation of the Luggin capillary to and from the electrode surface with corresponding iR bridge correction settings. The measurement of porous electrode performance curves involves a correction of the potential term which is often taken for granted, or treated casually. Since a potentiostat can control only the difference in potential between the tip of the reference probe and the working electrode, and not the working electrode metal/solution interface potential, the control potential contains an error due to the solution resistance. Under load, when current flows through the cell solution, a potential gradient occurs between the counter electrode and the working electrode. This gradient is caused by the resistance of the solution to ionic current flow. Due to this potential gradient the measurement of the solution/working electrode potential difference by direct means is impossible, since the reference probe cannot be located at the solution/working electrode interface without perturbing the interface and influencing the potential difference. Location of the reference electrode probe at a distance far enough away from the working electrode so that it does not disturb the potential difference means that the reference probe measures not only the working electrode/solution interface potential but also part of the potential gradient between the counter and working electrode when the cell is under load. The part of the potential gradient that the reference probe measures is referred to as the iR polarization or solution resistance.

Correction of the measured potential for the iR polarization can be accomplished by several methods and when data are reported to be "iR free or "iR corrected", one should know how that has been achieved and whether the procedure used is legitimate. Early automatic iR correction circuitry described by Kordesch and Marko (16) utilized a switching pulse derived from the

60 Hz line voltage. It is now recognized that this pulse frequency was too low to give adequate iR correction. Later, potentiostat circuits were designed employing positive feedback from the power output to the sensing circuits. Balance was achieved by driving the potentiostat into unstable oscillation and then backing off until the control circuits were stable. This procedure produces two results. The first is that an electrode under test is easily destroyed by the violent current and potential excursions during oscillation when maximum power of the potentiostat/galvanostat is applied. The second is that there is no criterion that indicates the iR term has been adequately neutralized.

In the rapid current interruption procedure with the electrode potential decay observed on an oscilloscope, the instantaneous potential decay reflects most of the iR in the solution but only to the outer face of the porous electrode. It does not correct for the iR within the porous electrode structure. The wide band bridge circuit used in the BC-1200 potentiostat does essentially the same thing as the current interruption technique, except that a small (±5 mA or ±5 mV) high speed square wave input (rise time 10 nano seconds) is followed by the potentiostat control circuits. If the rise time of the perturbing signal exceeds the response of the potentiostat, only the instrumental slew rate is measured, even though the current or potential step appears as an interruption to the potentiostat. In order for this technique to work, the potentiostat must have a very fast rise-time. The same waveform is observed under these conditions as would be seen with a physical circuit interruption. iR balance is achieved when the current/voltage perturbation is no longer observed by an oscilloscope.

Oxygen Reduction Activity

Activity data for reduction of 100% oxygen in 180°C, 100 w/o phosphoric acid were measured for several platinum on acetylene black carbon catalysts. Figure 7 shows performance curves for an electrode with 0.5 mg Pt/cm^2 loading. The solid points in the figure denote performance of baseline cells (17). Table 4 is a summary of the activity data. Analysis of the data is illustrated in Figures 8-10.

In Figure 8, the activity data at 800 mV and 900 mV are compared. There is an apparent crystallite size effect based on the least squares fit of the data. However, visual inspection of the data suggests that one line could adequately fit all the data as well.

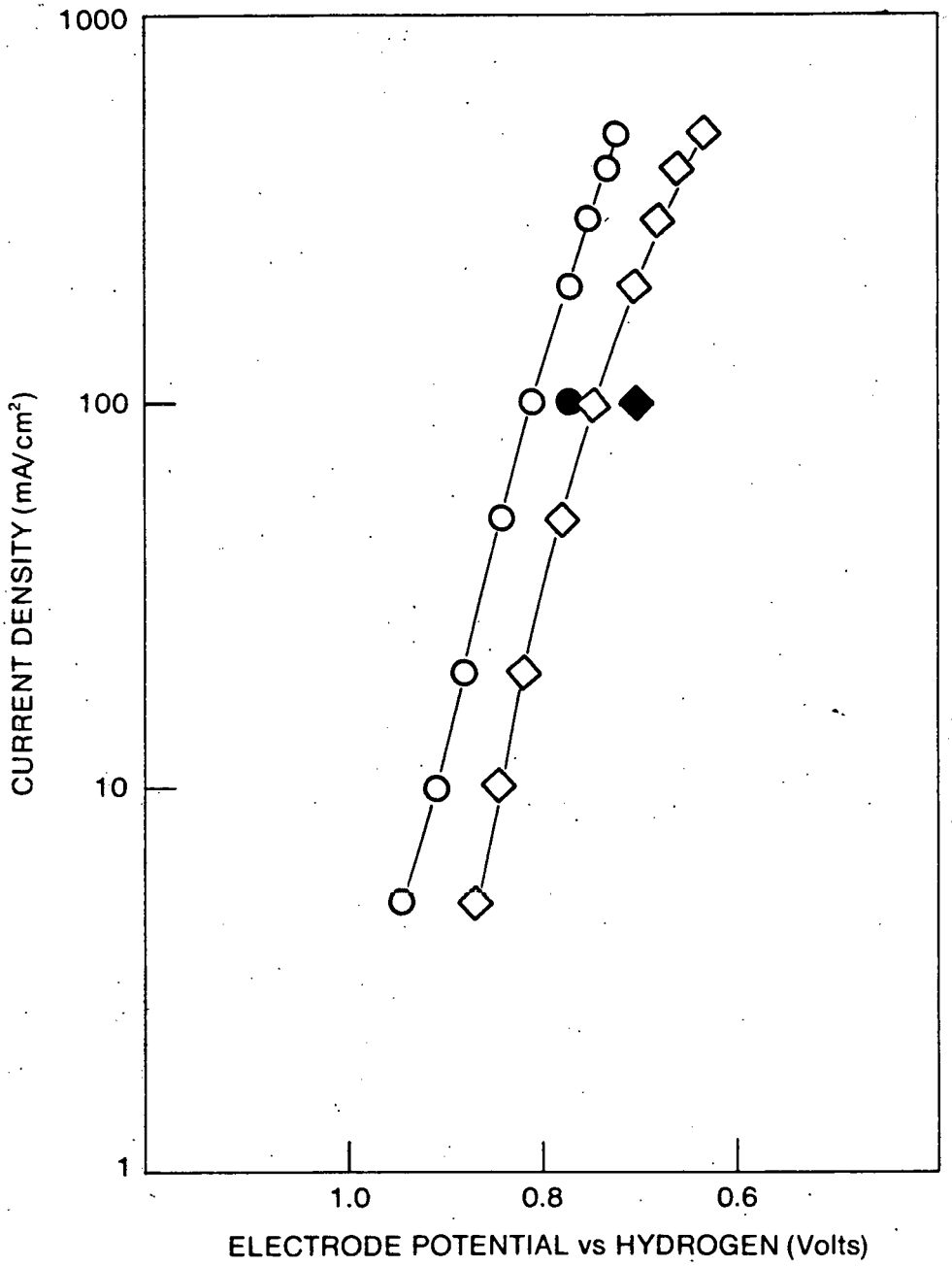

Figure 7. Performance curves on O_2 (●) and on air (◆) for an improved electrode structure in the half-cell apparatus at 180°C in 102 w/o H_3PO_4; electrode loading 0.5 mg Pt/cm^2 as 10 w/o Pt on Vulcan XC-72R. The solid points baseline performances from Ref. (17).

Table 4: Electrocatalyst Activity Data

Catalyst	Platinum Loading (mg/cm^2)	Post Test Platinum Surface Area (m^2/gm)	Catalyst Layer Thickness (μm)	Activity @ 900 mV ($\mu A/cm^2$ Pt (O_2))	Activity @ 800 mV ($\mu A/cm^2$ Pt (O_2))
1% Pt/Shawinigan	0.05	68	130	18	231
5% Pt/Shawinigan	0.50	76	130	13	126
5% Pt/Shawinigan	0.25	77	65	20	231
10% Pt/Shawinigan	0.5	55	130	24	210
10% Pt/Shawinigan	0.5	64	130	34	259
15% Pt/Shawinigan	0.5	56	85	34	245
15% Pt/Shawinigan	0.75	54	130	40	312
20% Pt/Shawinigan	0.5	49	65	42	344
20% Pt/Shawinigan	1.0	49	130	41	277
10% Pt/Shawinigan	0.5	61	130	34	313
10% Pt/Shawinigan 400°C HT	0.5	65	130	21	257
10% Pt/Shawinigan 941°C HT	0.5	46	130	42	363

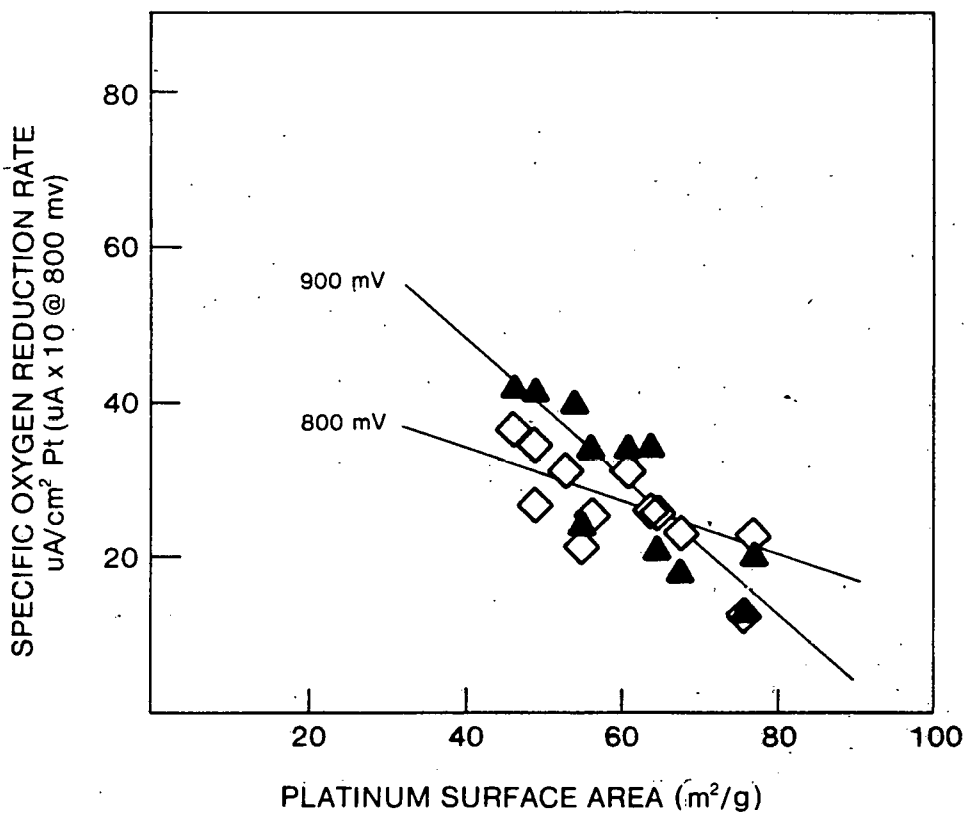

Figure 8. Specific oxygen reduction rate as a function of surface area at 180°C in 100 w/o H_3PO_4.

The activity data of Bregoli (1) are plotted in Figure 9 along with the data obtained at 900 mV platinum on acetylene black. Bregoli's data were taken for platinum on Vulcan XC-72 and platinum black. The apparent crystallite size effect exhibited by catalysts supported on Vulcan and platinum black is different from that exhibited by catalysts supported on acetylene black. This implies that the measured activity for oxygen reduction is dependent on the substrate used to support the catalyst.

An alternative argument for the apparent crystallite size effect is that the observed decrease in specific activity with increase in surface area is due to\diffusion effects. As the surface area of the electrocatalyst increases, the turnover number approaches a rate whereby reactant cannot be supplied to the crystallite at a comparable rate. Hence, the active metal is not effectively utilized and performance is limited by diffusion. This diffusion phenomena produces an observed decrease in specific activity with increase in surface area.

Kunz and Gruver (18) derived electrochemical rate equations for gas diffusion electrodes operating under activation control or under diffusion control. These equations resulted in the current at a given potential varying linearly with catalyst loading if the electrode operates in the kinetic control regime and with the square root of catalyst loading if the electrode operates in the diffusion control regime. It was therefore suggested that the controlling regime could be determined by varying the catalyst loading. Two caveats exist, however. The first is that the specific surface area may change with loading so it is more correct to use the platinum surface area instead of the platinum loading. This was done for the data reported in Table 4. The current/surface area relationship is shown in Figure 10. A least squares analysis results in an approximately linear variation suggesting that the electrodes operate under kinetic control. The second caveat is the validity of the criterion for applicability of the diffusion control rate equation derived by Kunz and Gruver -- which is not clear. The criterion for applicability is that the parameter

$$\frac{R_a}{2}\left\{\frac{SWi_o\tau \exp(\alpha nF\eta/RT)}{nFLD_{O_2}\alpha_{O_2}\varepsilon}\right\}^{\frac{1}{2}}$$

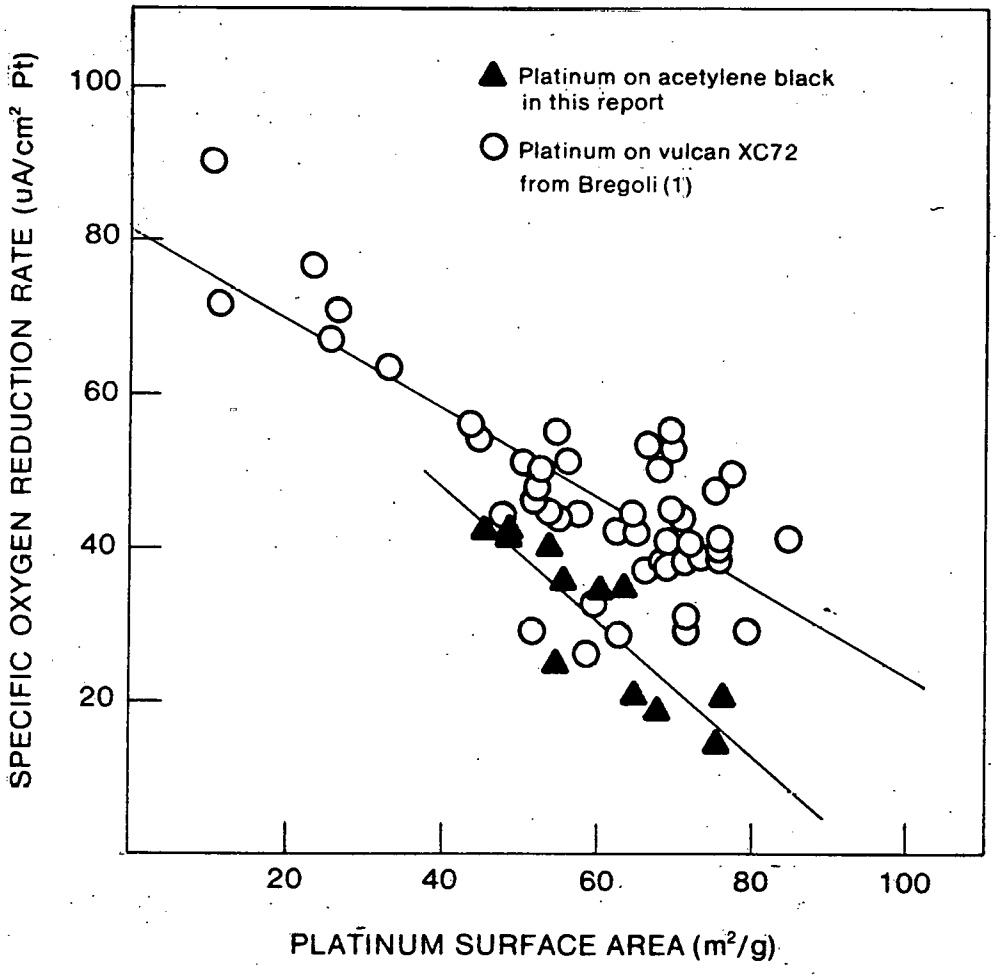

Figure 9. Specific oxygen reduction rate as a function of surface area at 180°C in 100 w/o H_3PO_4 at 900 mV.

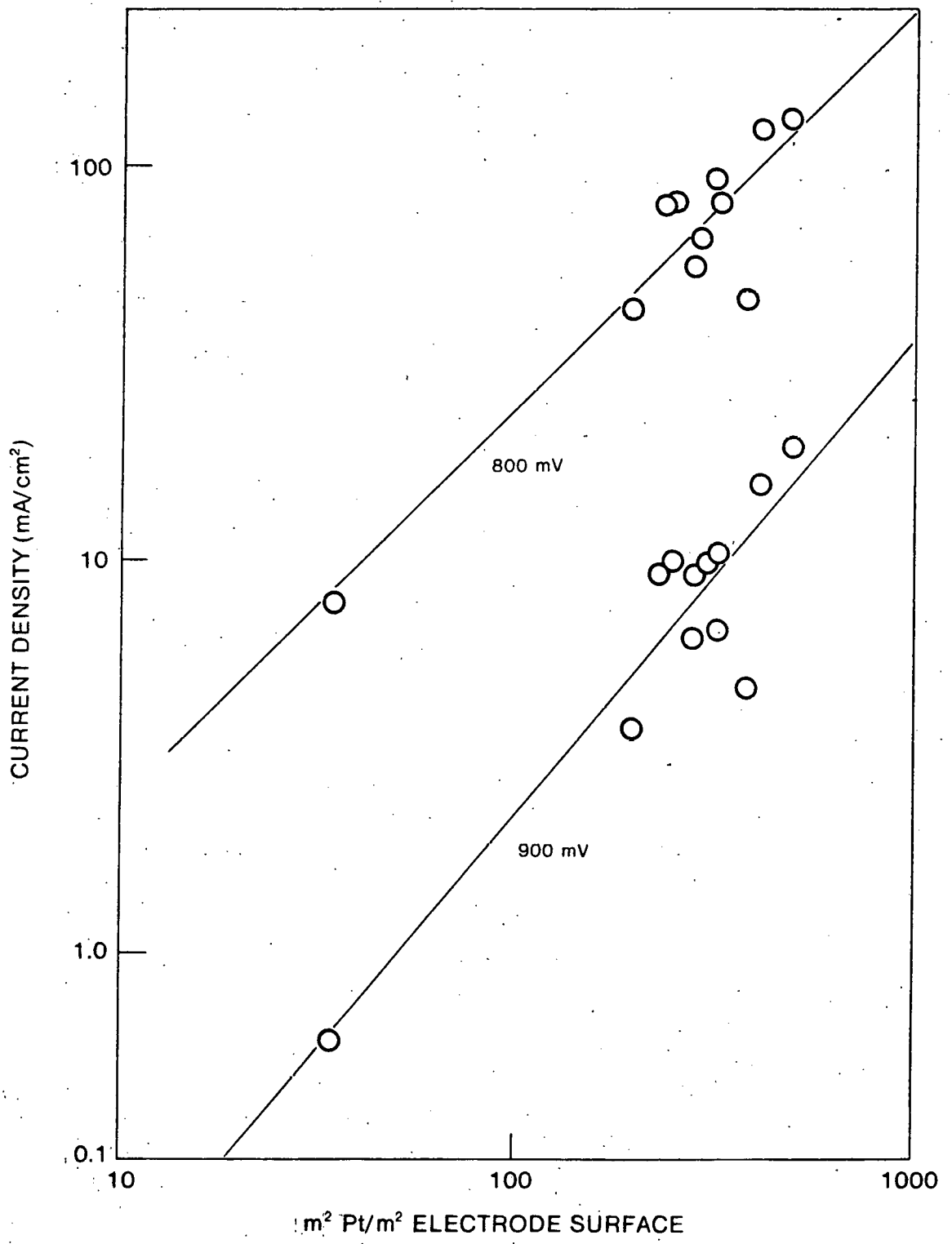

Figure 10. Variation of current density with Pt surface area for Pt supported on acetylene black at 180°C in 100 w/o H_3PO_4 on O_2.

is "large". Here, R_a is the agglomerate radius in cm, L is the electrode thickness in cm, W is the platinum loading in g/cm^2 frontal area, S is the platinum surface area in cm^2/g, τ is the agglomerate tortuosity, $D_{O_2}\alpha_{O_2}$ is the oxygen diffusivity-solubility product in mole/cm-sec., ε is the agglomerate porosity, i_o is the exchange current density in A/cm^2 Pt, and the remaining terms have their usual electrochemical definitions. Numeric limits were not specified. Using the electrode properties in Table 4 and data specified by Kunz and Gruver, the criterion for the electrodes used in this work is only on the order of 5 or less. Hence, the square root relationship may not be valid.

Apparent activation energies for oxygen reduction were estimated from the temperature effect on the polarization curves. The data shown in Figure 11 are for an electrode containing 0.53 mg Pt/cm^2 electrode and operating on air. The post test surface area of the platinum was 30 m^2/g based on electrochemical adsorption measurements. The PTFE loading was 30 w/o, and the carbon support was Shawinigan acetylene black. The temperature range investigated was 139-228^{o}C. All measurements were iR compensated. The data compare favorably to previously reported performance results (18,19) as seen in Figure 12.
The data reported in Figure 11 cannot be used directly to extract kinetic information since they do not account for the change in the theoretical open circuit potential (TOCP) of the oxygen electrode with temperature. The overall reaction which occurs in the cell is:

$$O_2 + 2H_2 \rightarrow 2H_2O \qquad \text{Equation (3)}$$

The reversible Nernst potential for this reaction is:

$$E = E_o^T + \frac{RT}{4F} \ln \left\{ \frac{P^2_{H_2O}}{P_{O_2} P^2_{H_2}} \right\} \qquad \text{Equation (4)}$$

where:

$$2FE_o^T = 57{,}410 + 0.94T\ln T + 3.92T + 0.00165T^2 - 3.7 \times 10^{-7} T^3 \qquad \text{Equation (5)}$$

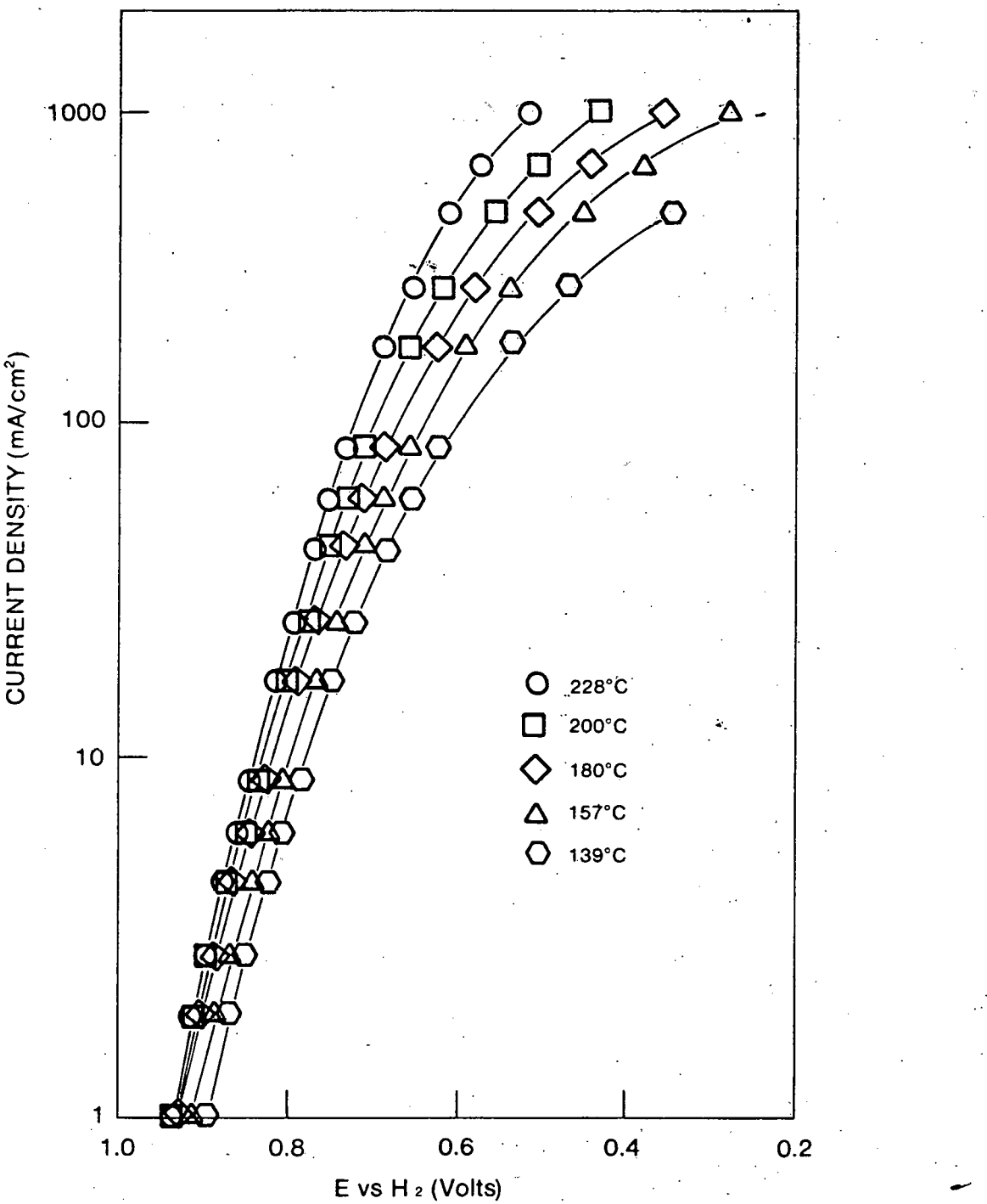

Figure 11. Performance curves for oxygen reduction at various temperatures. Electrode run on air at 1 ohm in 104.6 w/o H_3PO_4. Electrode is 0.53 mg Pt/cm^2 (30 m^2/g post test analysis) on Shawinigan acetylene black, with 30% Teflon.

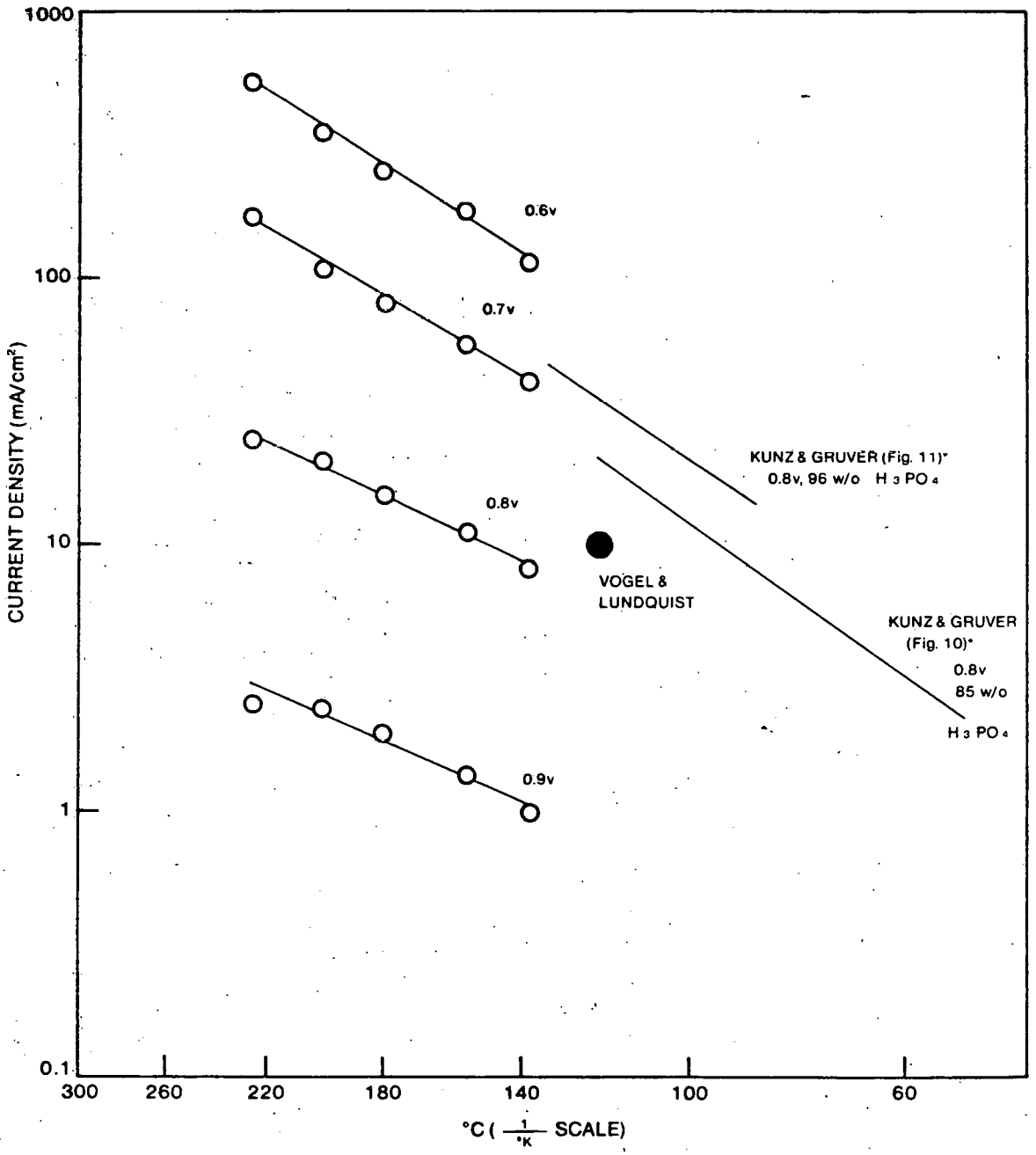

Figure 12. Current density as a function of 1/T for various potentials. In 104.6 w/o H_3PO_4.

To understand the effect of temperature on the oxygen reduction electrode kinetics, it is necessary to generate information on the partial pressure of water in concentrated acids as a function of temperature. The closest information is that given by MacDonald and Boyack (20). Their data are reported for temperatures between 130°C and 170°C and for phosphoric acid concentrations in the range 75-102 w/o. An empirical correlation was developed for these conditions. This correlation was used to extrapolate to 104.6 w/o acid and 250°C. Results are reported in Figure 13. The water vapor pressure can then be used in Eqn. (4) to estimate the theoretical open circuit potential for the oxygen reaction. The results for oxygen are reported in Figure 14. Identical calculations can be performed for air.

To determine the real activation energy for oxygen reduction, it is necessary to know the exchange current density for the reaction. The exchange current density is obtained by extrapolating the Tafel slope out to the theoretical open circuit potential. Appleby has done this and reported a value of 22 k.cal/mole (21) for oxygen reduction on smooth platinum. Others (18,19) have measured oxygen reduction on platinum black and platinum on carbon and extrapolated the polarization curves back to the theoretical open circuit potential to obtain values close to 22 k.cal/mole.

Two assumptions are made to obtain the activation energy by extrapolation to the open circuit potential. First, in the Nernst equation, it is assumed that the reversible potential can be accurately calculated at elevated temperature and that the partial pressures of oxygen, hydrogen, and water vapor can be used instead of their activities. Since the vapor pressure data above 170°C and 102 w/o H_3PO_4 were extrapolated, some doubt exists as to the accuracy of these estimates. The second assumption is that performance curves can be extrapolated to the open circuit potential along an experimentally determined Tafel slope. This procedure is difficult because the performance curves often do not exhibit linearity over a large range of potentials to permit an unequivocal Tafel slope determination. Kunz and Gruver (18) report a Tafel slope of 90 mV/decade at 160°C and equate this to 2.3 RT/F.

An alternative procedure can be developed to estimate activation energies. The electrochemical reaction rate is:

$$i = i_o \exp\left(-\frac{\beta n F \eta}{RT}\right) \qquad \text{Equation (6)}$$

where

$$i = k_o C \exp\left(-E/RT\right) \qquad \text{Equation (7)}$$

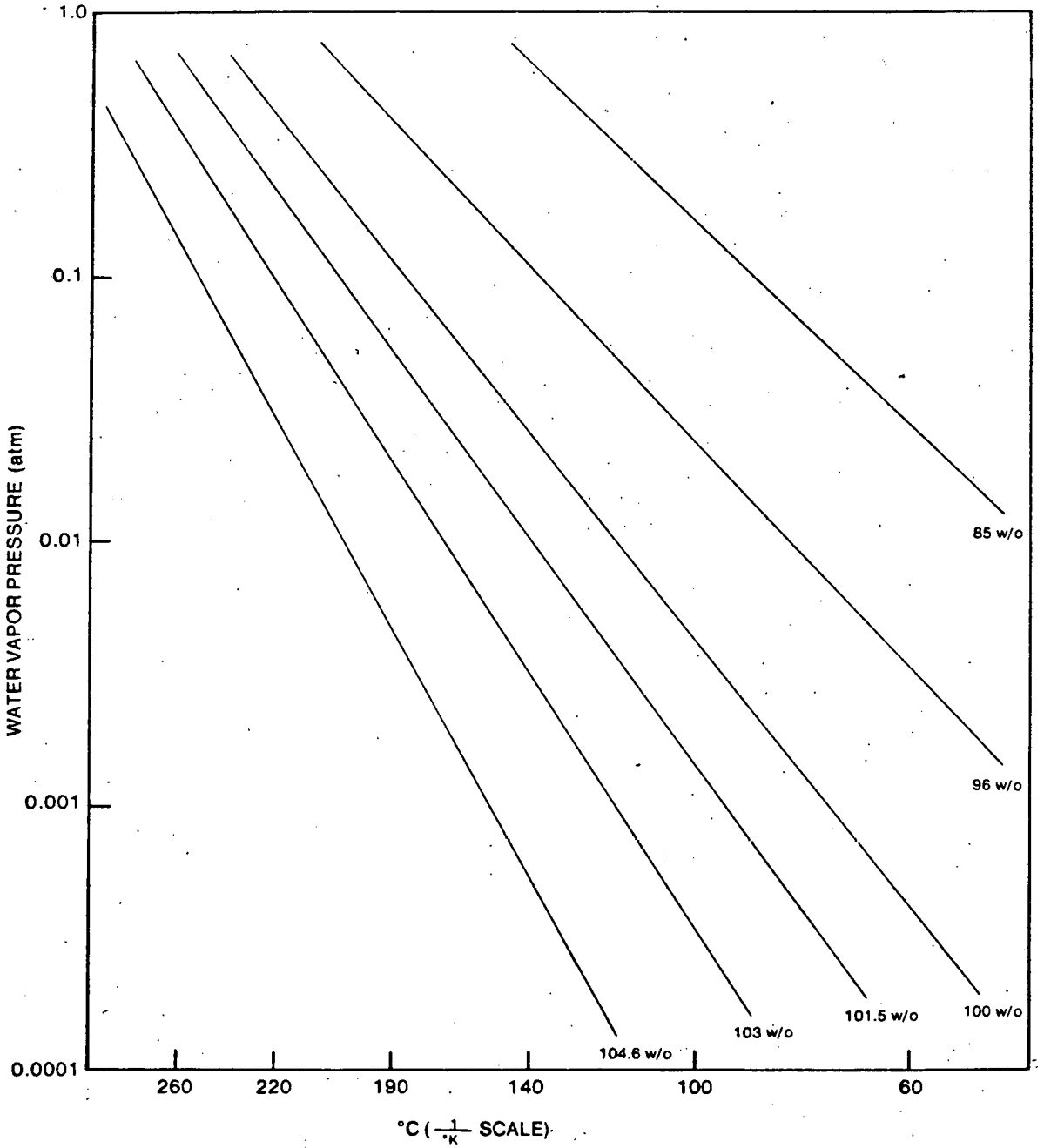

Figure 13. Water vapor pressure over concentrated phosphoric acid at various acid concentrations as a function of 1/T.

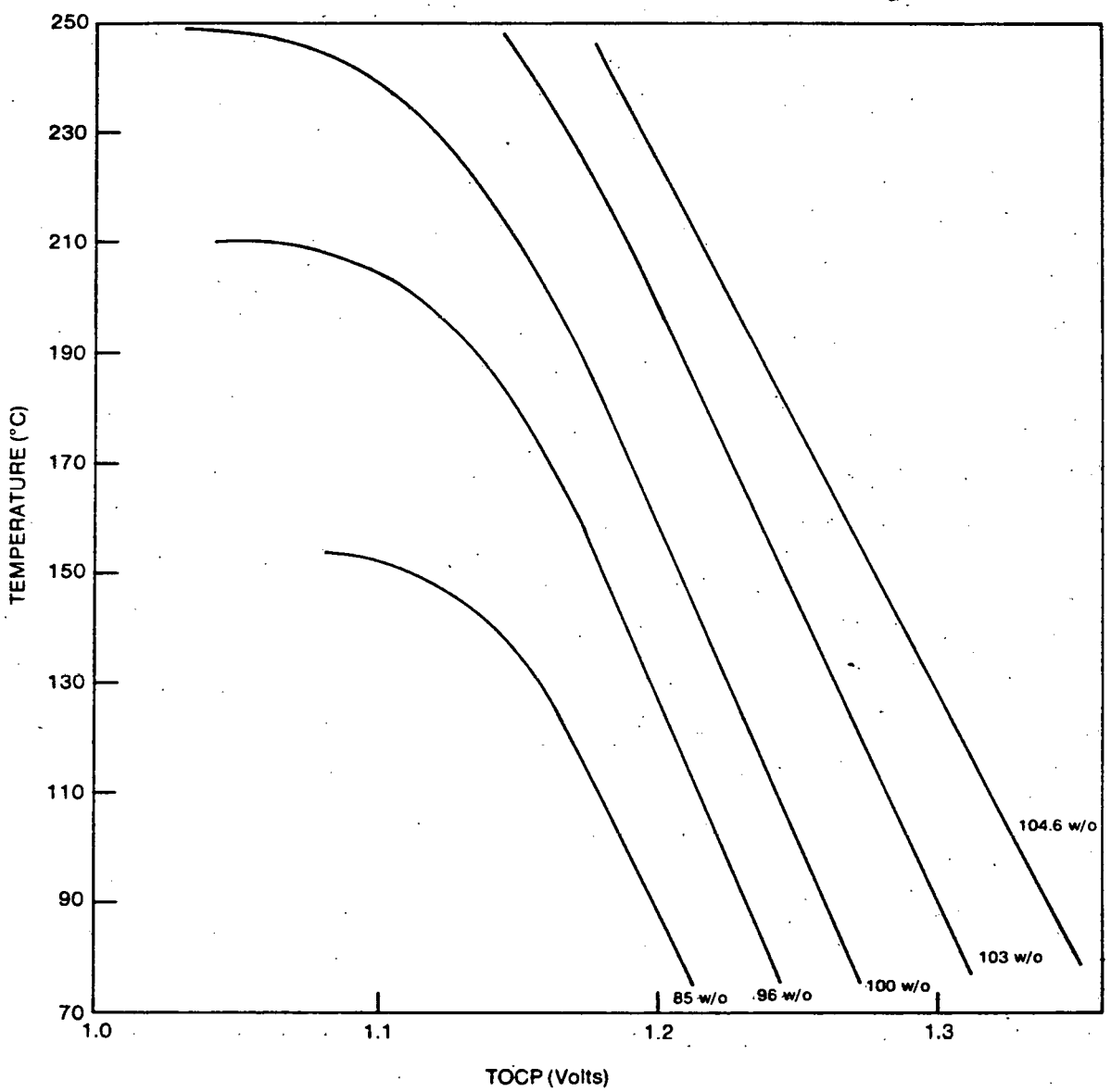

Figure 14. Change in the theoretical open circuit potential with temperature for various acid concentrations.

In Eqn. (7), E is the activation energy at zero overpotential, i.e. the standard chemical activation energy. Extrapolation to the open circuit potential gives the exchange current density which can then be used to estimate E. The exchange current density, i_o, thus the reaction rate, is suitably small so that the concentration term, C, remains unchanged. It is clear that activation energy estimates can be made at any overpotential provided that both the overpotential and the concentration terms are essentially constant.

For the experiments reported in Figure 11, about 3.12×10^{-5} g mole O_2/sec are introduced to the electrode. At 1 amp/cm^2 2.59×10^{-6} g mole O_2/sec are turned over. This represents a maximum oxygen conversion of only about 8%. As a result, the approximation of constant concentration can be used. The Arrhenius plot then takes the form:

$$\ln i = \ln K - \{ \frac{E}{R} + \frac{\beta n F}{R} \eta \} \frac{1}{T} \qquad \text{Equation (8)}$$

so that the activation energy can be estimated from:

$$E = mR - \beta n F \eta \qquad \text{Equation (9)}$$

where m is the Arrhenius slope, and E is in joules/mole ^oK.

The data of Figure 11 were corrected for changes in the theoretical open circuit potential and these results are reported in Figure 15. Figure 16 is the Arrhenius representation at 300, 400, and 500 mV overpotential. A least squares analysis yields Arrhenius slopes of approximately 6.7×10^3 ^oK at each overpotential. The activation energies at each overpotential were estimated using Eqn. (9). The results are reported in Table 5. Based on results from previous work (17,19,21), diffusion control is indicated. If the data in Figure 15 are extrapolated to the theoretical open circuit potential along an assumed Tafel slope of 2.3 TR/F, an activation energy of 25 k.cal/mole is obtained. This value is about twice that obtained using Eqn. (9) at zero overpotential. It has been shown that for the case where diffusion factors control the rate of reaction, the apparent activation energy is about one-half the activation energy obtained when kinetic factors dominate (22). The correspondence to electrocatalysis has been pointed out previously (23). This phenomenon has a direct analog in flooded agglomerate pore theory.

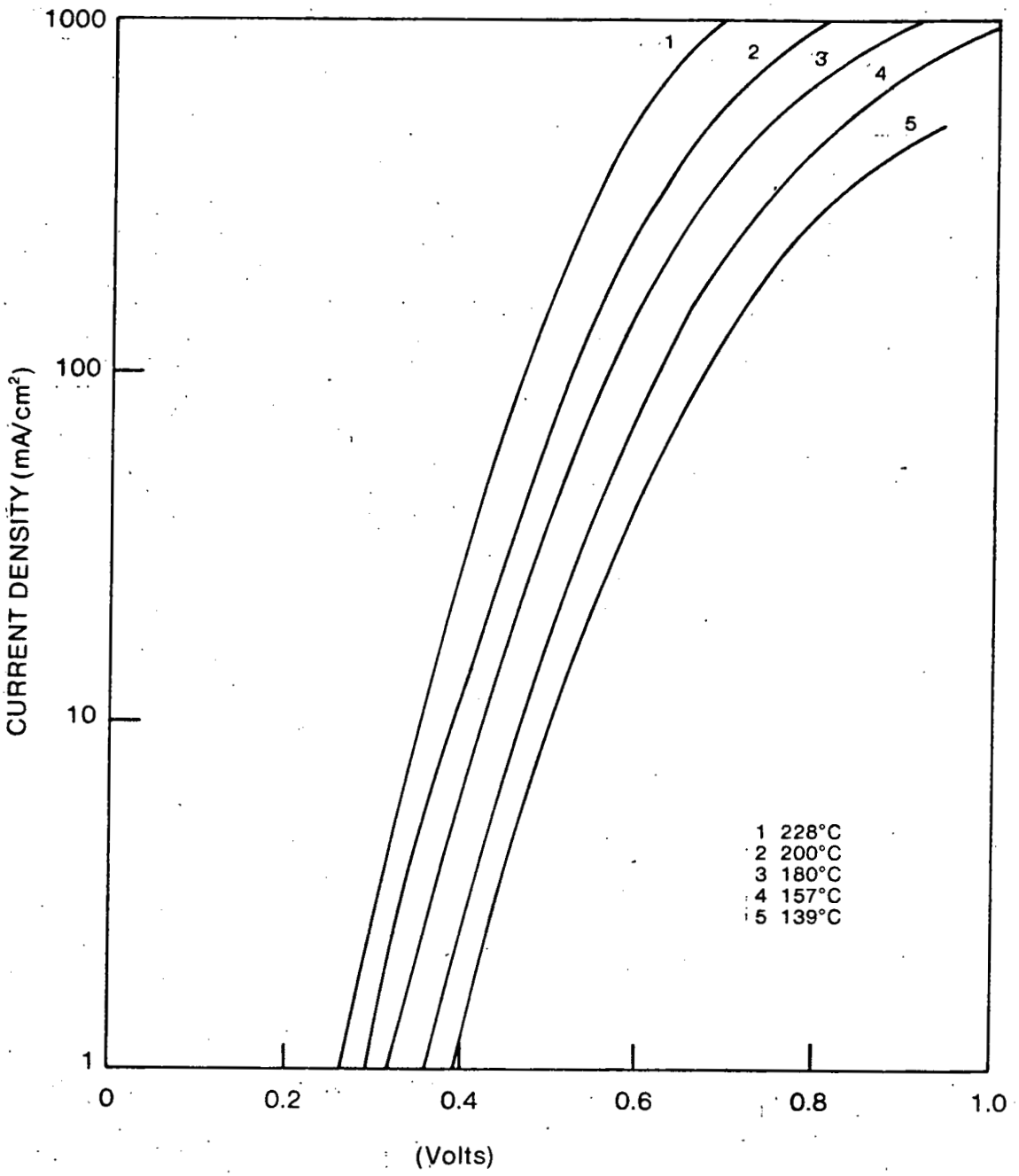

Figure 15. Current density as a function of overvoltage for oxygen reduction at various temperatures. Electrode is 0.53 mg Pt/cm^2 on acetylene black with 30% TFE run on air in 104.6 w/o H_3PO_4.

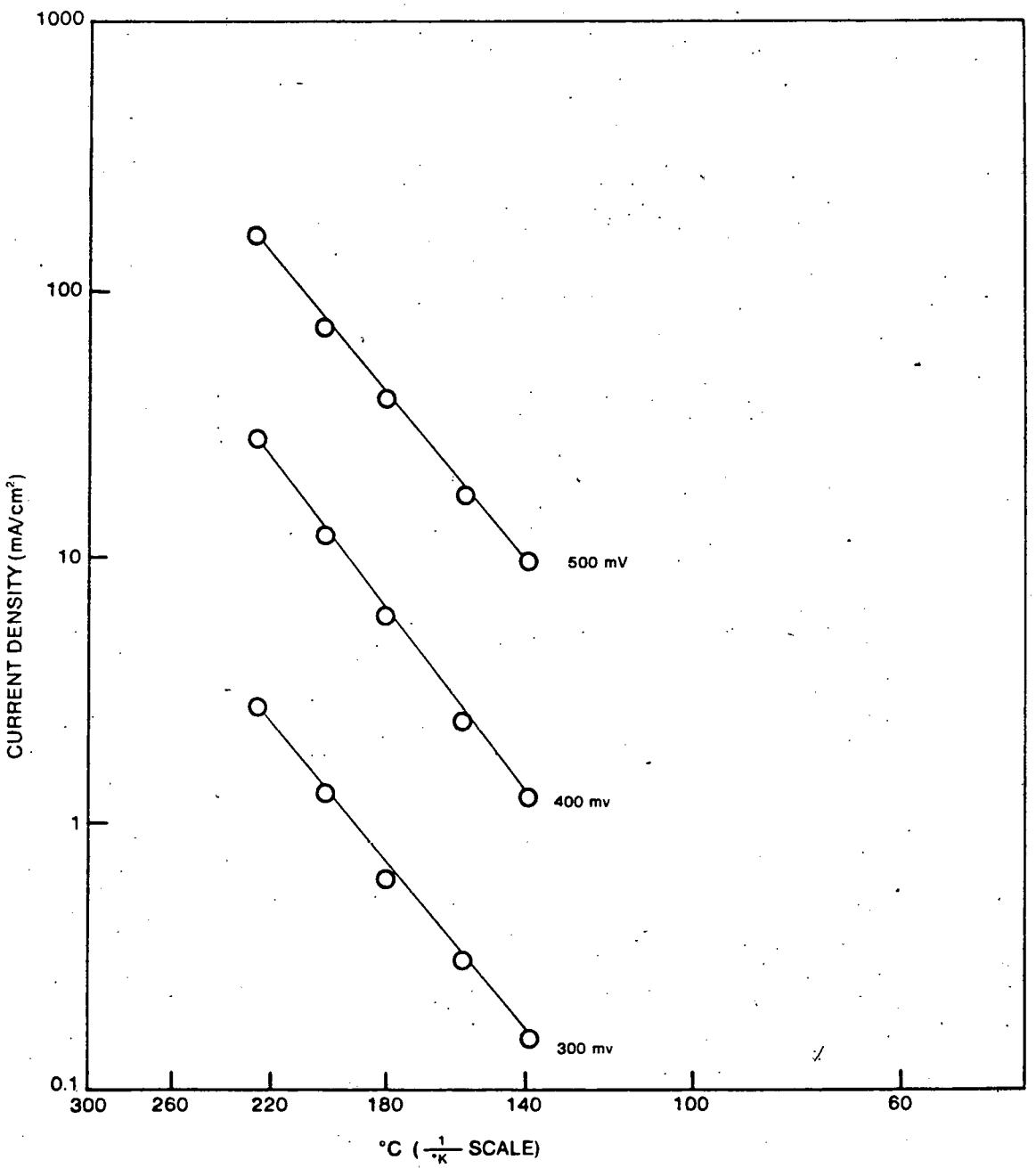

Figure 16. Current density as a function of 1/T for various overvoltages.

Table 5: Apparent Activation Energies for Oxygen Reduction

η, V	E, k.cal/mole
0	13.3
.3	9.86
.4	8.68
.5	7.54

Hydrogen Oxidation Activity

Electrodes were prepared by the procedure outlined in the experimental section for each electrocatalyst listed in Table 1. The hydrogen oxidation characteristics of these electrodes were determined. Since the rate of hydrogen oxidation reaction on platinum is very fast, the electrode structures probably operate in a diffusion controlled mode. Polarization data were obtained over the temperature range 125-240^{o}C. A representative set of polarization curves is shown in Figure 17. These data were used to construct Arrhenius plots at 25, 50 and 100 mV polarization in Figure 18. The Arrhenius slopes for operation on hydrogen (shown as the continuous line in the figure) were constant at about 4 x 10^{3} ^{o}K. Analysis similar to that employed for the oxygen data can be used. The hydrogen conversions at 1 amp/cm^{2} are on the order of 2-4% so the hydrogen concentration term can be assumed constant. It must also be assumed that the hydrogen surface coverage remains essentially constant over the range of temperatures investigated. Based on the work of Ferrier, et al. (24), this is a reasonable assumption for the experimental conditions employed. A decrease in the apparent activation energy is observed as indicated in Table 7. Clearly, the electrode is operating in a diffusion controlled regime. Improved performance can therefore be realized by development of better electrode structures.

It was found that lowering the Teflon content from 50 w/o to 40 w/o improved the performance. Figure 19 shows the performance curve for the best of these electrodes. Arrhenius plots at 25 and 50 mV were linear and approximately parallel as shown by the open circles in Figure 20. The Arrhenius slope was estimated to be about 4.5 x 10^{3} ^{o}K using least squares resulting in somewhat higher apparent activation energies. Comparison of these values with those obtained from the data in Figure 18 is shown in Table 7. The apparent activation energy indicates that the diffusion characteristics of the electrode have been improved.

As pointed out in a previous section, the variation of the standard chemical activation energy is indicative of diffusion controlled operation. Even though the electrodes tested in this work are diffusion controlled, improved structure can be realized thereby improving electrode performance.

Hydrogen Oxidation Poisoning by CO

The effect of carbon monoxide as a site specific poison for electrocatalysis of the hydrogen oxidation reaction using the platinum electrocatalysts prepared in this program was also investigated.

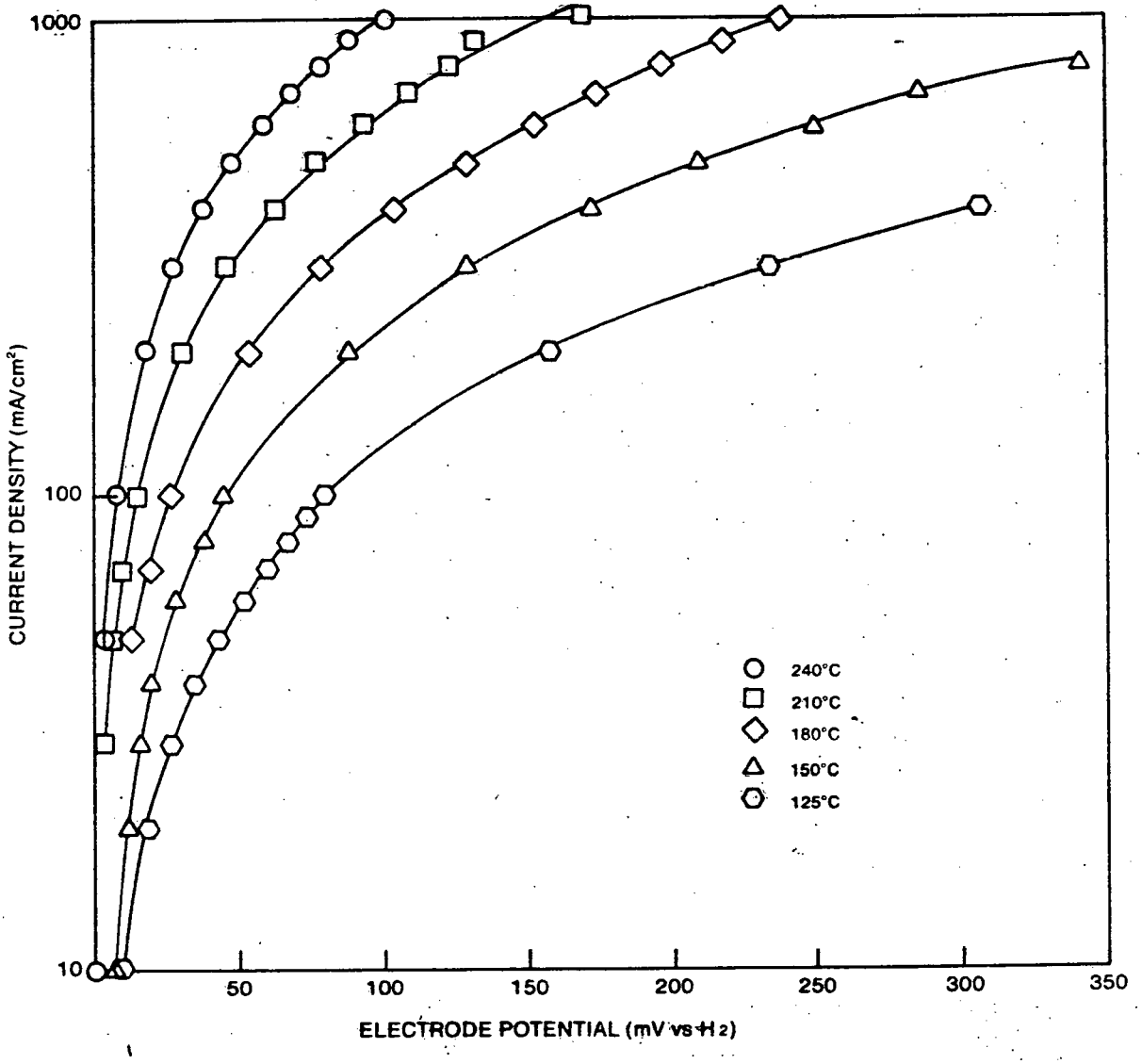

Figure 17. Polarization curves for hydrogen oxidation at various temperatures in 104.5 w/o H_3PO_4. Catalyst is 10% platinum on Vulcan. Electrode is 50% catalyst/50% Teflon, 0.25 mg Pt/cm^2. Post test platinum surface area is 58 m^2/gm.

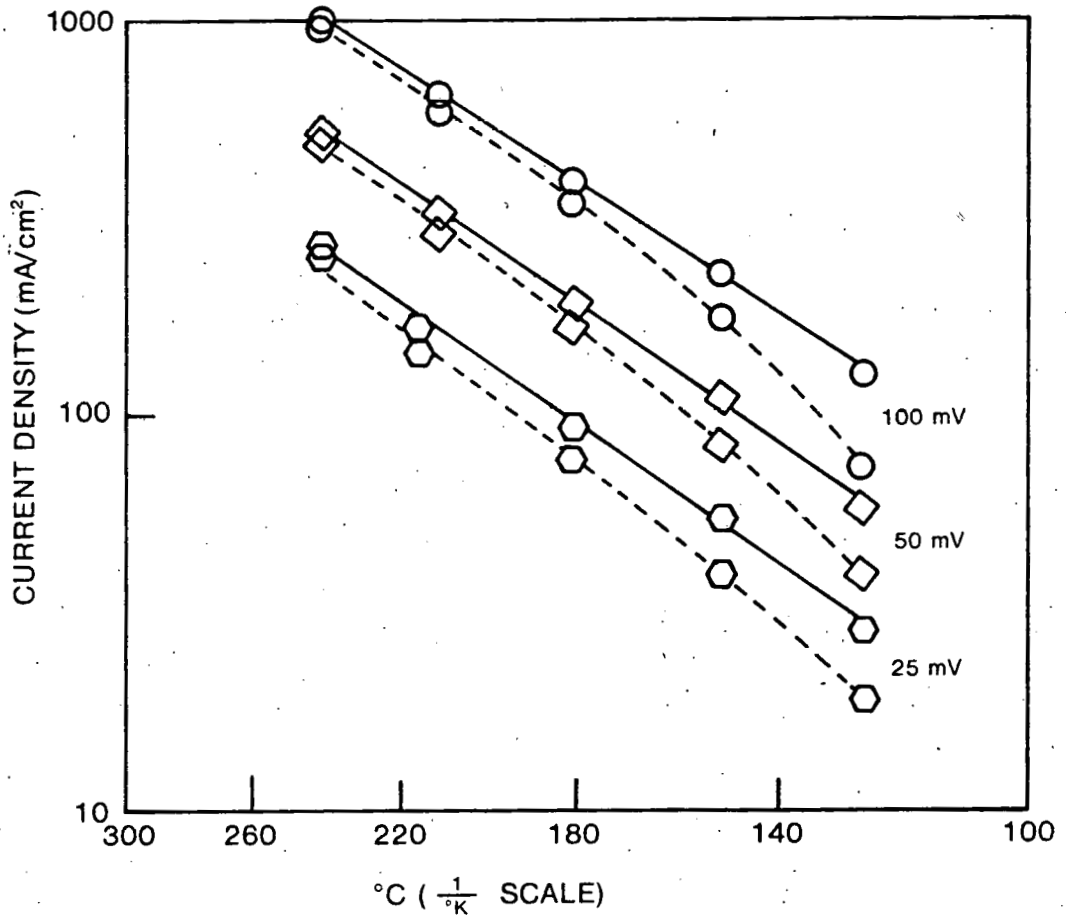

Figure 18. Current density as a function of temperature for hydrogen oxidation on 100% H_2 —— and 2% CO/H_2 ---- at 25, 50 and 100 mV polarization, in 104.5 w/o H_3PO_4. 0.25 mg Pt/cm^2, 10% Pt/Vulcan, 50% PTFE.

Table 7: Apparent Activation Energies for Hydrogen Oxidation

η, V	E_{app} (50%)	E_{app} (40%)
0	7.69	9.0
.025	7.11	8.45
.05	6.53	7.86
.10	5.38	--

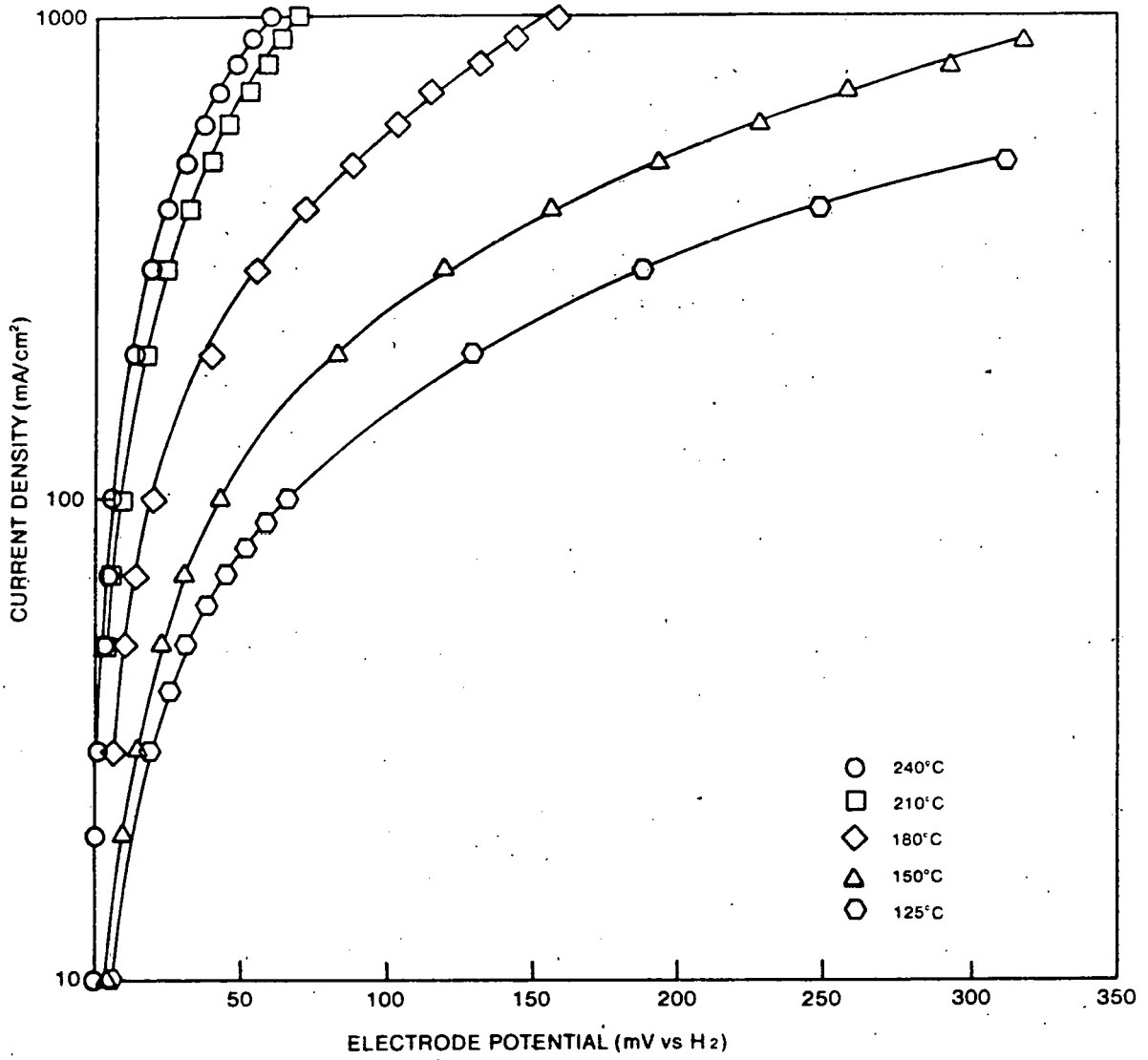

Figure 19. Polarization curves for hydrogen oxidation at various temperatures in 104.5 w/o H_3PO_4 catalyst in 10% platinum on Vulcan. Electrode in 60% catalyst/40% Teflon, 0.25 mg Pt/cm^2. Post test platinum surface area is 52 m^2/gm.

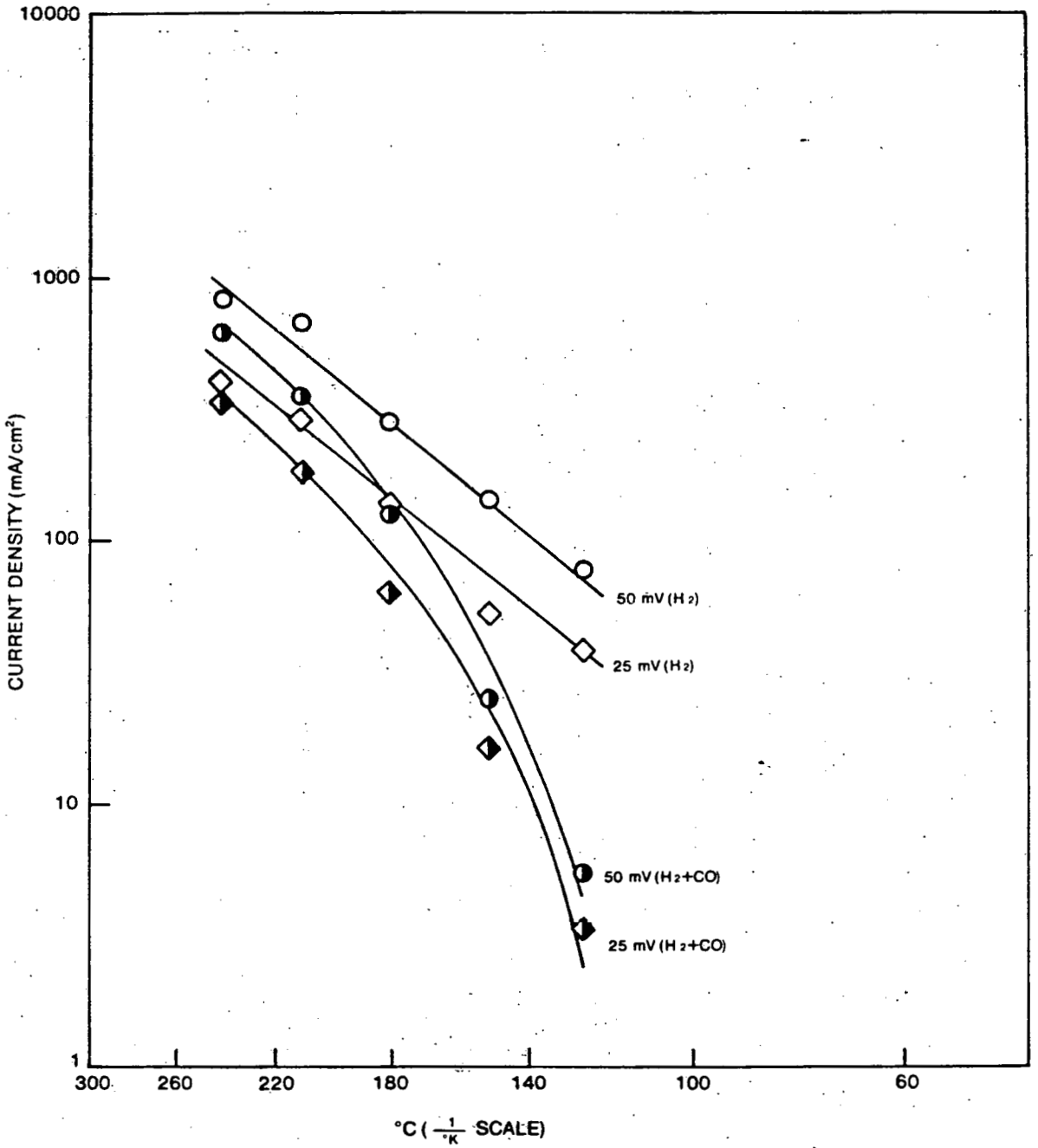

Figure 20. Current density as a function of temperature for hydrogen oxidation on 100% H_2 and H_2 + 30% CO, at 25 and 50 mV polarization, in 104.5 w/o H_3PO_4. 0.25 mg Pt/cm^2, 10% Pt/Vulcan, 40% PTFE.

The electrode structures used to obtain the data shown in Figure 17 and Figure 19 were subjected to a fuel gas stream of hydrogen containing 2% carbon monoxide. Polarization curves were run as before over the temperature range 240°C to 125°C. The data are shown in Figure 21 and should be compared to the curves shown in Figure 17. Apparent activation energy plots were obtained for 25, 50, and 100 mV polarizations. These values also are plotted in Figure 18 as the dashed lines. At the highest temperatures there is a very small decrease in the hydrogen oxidation activity. This means that the carbon monoxide surface coverage is low and only a small part of the platinum surface is covered by this poison. At lower temperatures, however, the poison coverage increases. If methanol is considered as a primary hydrogen fuel source for fuel cells, thermal cracking results in a mixture containing a 2/1 ratio of H_2/CO. Performance curves were, therefore, obtained for fuel streams containing 30% carbon monoxide. These polarization curves are shown in Figure 22. It can be seen that at temperatures up to 150°C the fuel cell electrocatalyst is incapable of running at the 100 mA/cm^2 level. Corresponding pseudo Arrhenius plots are shown in Figure 20 as the filled symbols so that a comparison can be made with hydrogen oxidation values in the presence and the absence of carbon monoxide but the same partial pressure of hydrogen. At the higher temperatures carbon monoxide adsorption results in a relatively small decrease in performance for hydrogen oxidation. At lower temperatures, however, appreciable carbon monoxide coverages are attained resulting in a dramatic performance decrease.

There is one further extension that the poisoning data provides. By comparison of the current density for hydrogen oxidation in the absence of carbon monoxide to that current density obtained for hydrogen oxidation in the presence of carbon monoxide, the carbon monoxide coverage as a function of temperature and partial pressure can be estimated. The results for the 2% and the 30% carbon monoxide level are shown in Figure 23. At the 30% carbon monoxide level and 125°C, over 90% of the platinum surface is covered by carbon monoxide. At the same carbon monoxide level and 240°C, only 25% of the surface is covered by carbon monoxide.

If a Langmuir isotherm is assumed:

$$\theta = \frac{Kp}{1 + Kp} \qquad \text{Equation (10)}$$

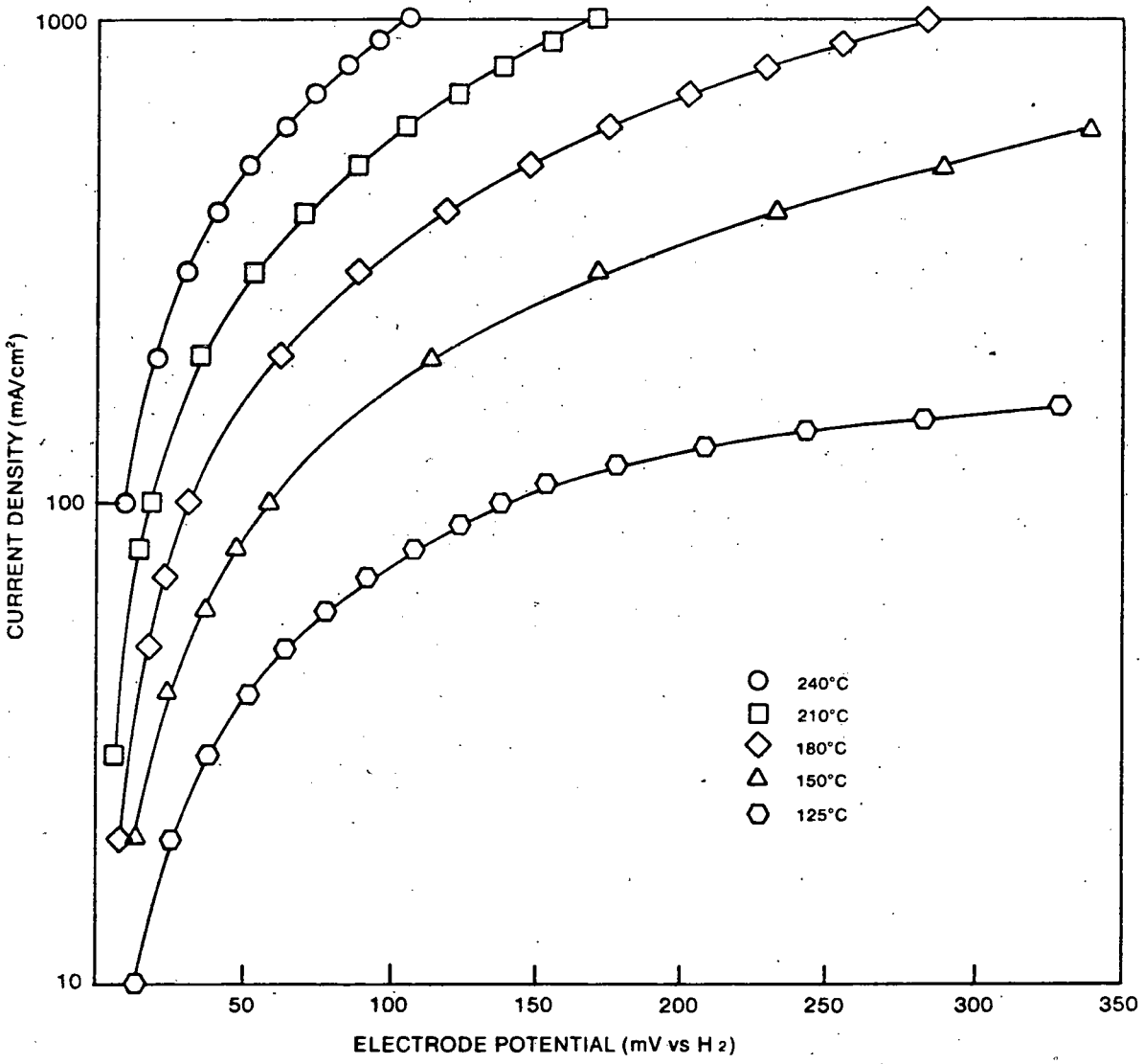

Figure 21. Polarization curves for hydrogen oxidation with 2% CO in fuel gas at various temperatures in 104.5 w/o H_3PO_4. 10% Pt/Vulcan, 0.25 mg Pt/cm^2, 50% PTFE.

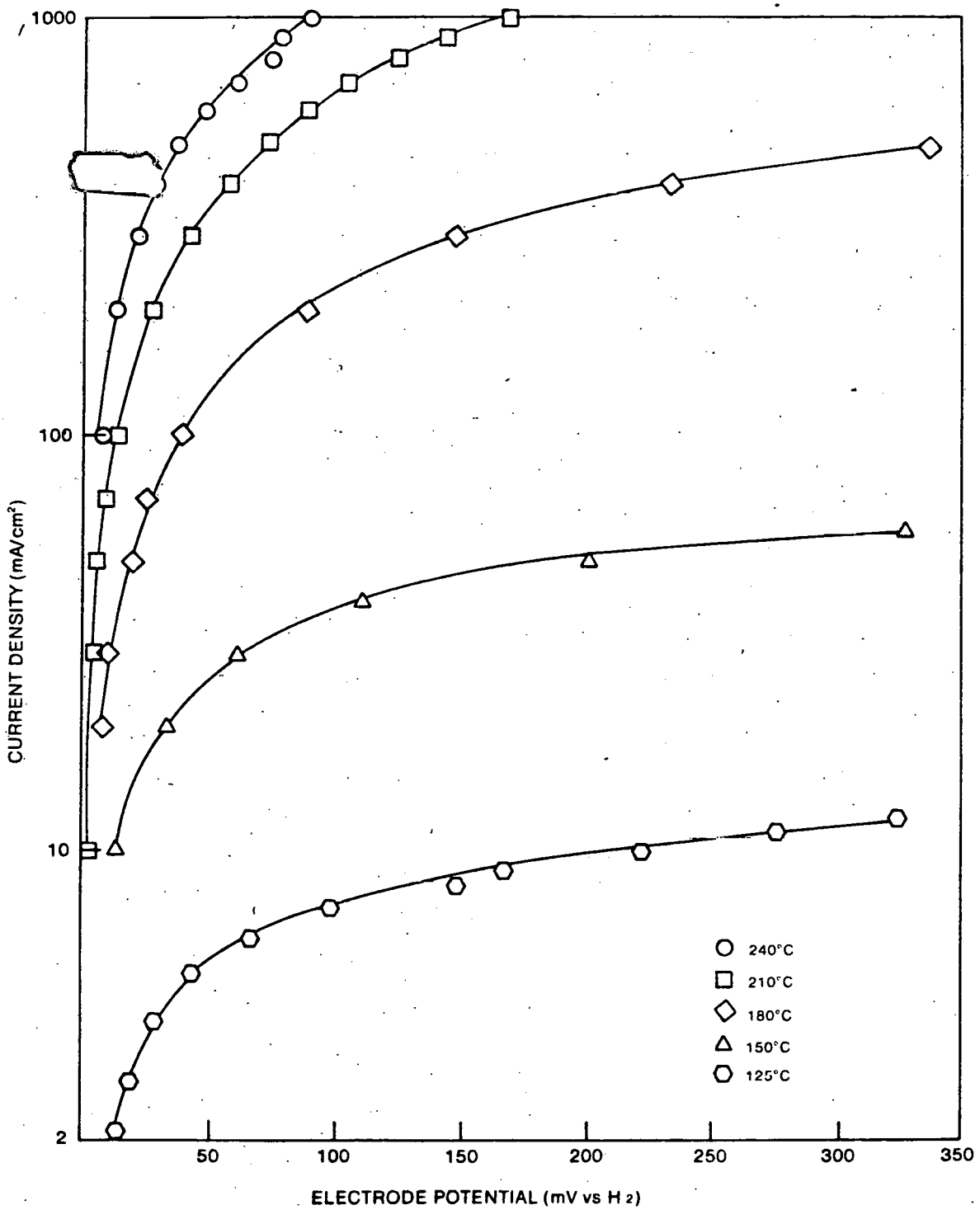

Figure 22. Polarization curves for hydrogen oxidation with 30% CO in fuel gas at various temperatures in 104.5 w/o H_3PO_4. 10% Pt/Vulcan, 0.25 mg Pt/cm^2 40% PTFE.

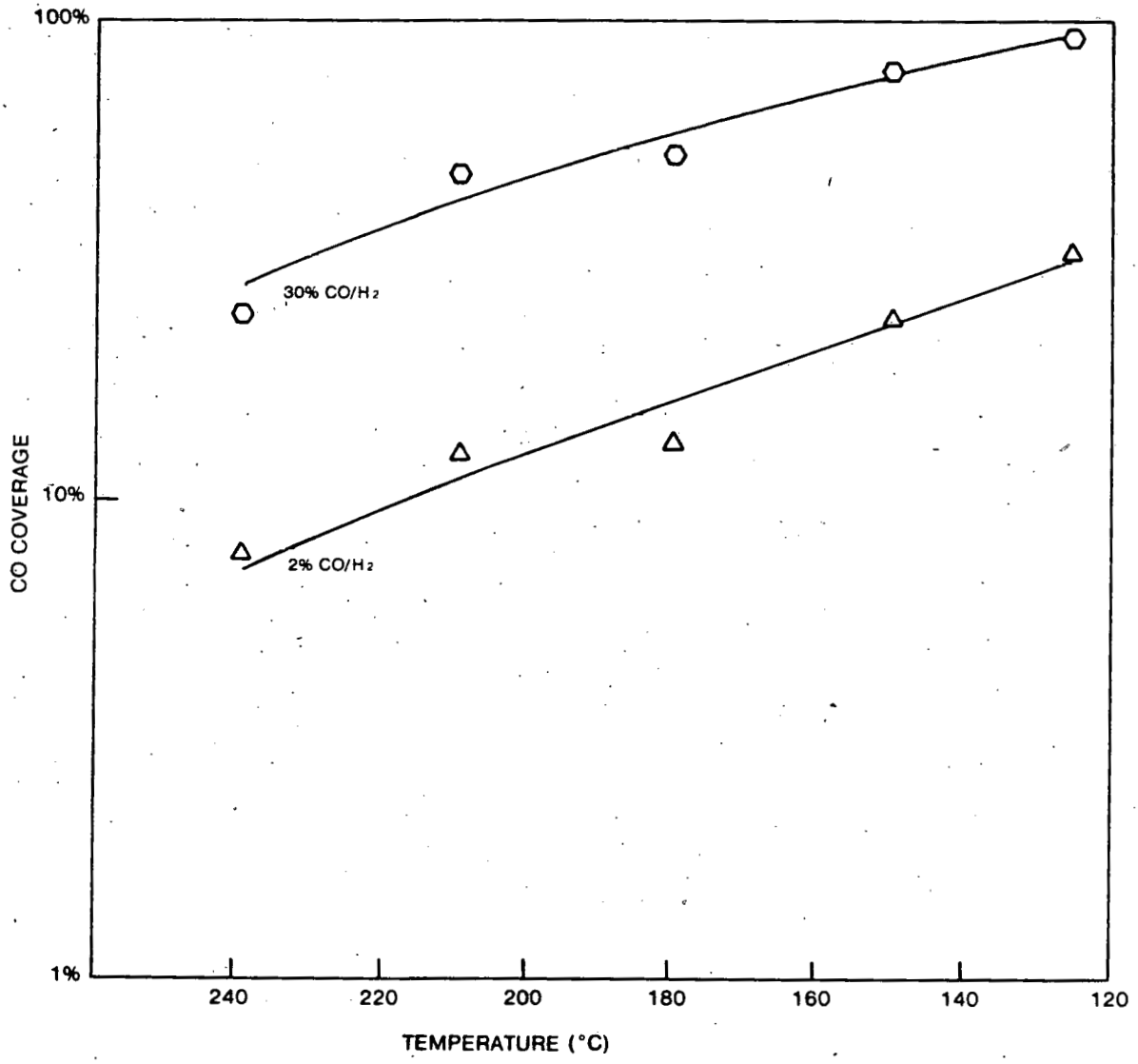

Figure 23. Percentage of platinum surface covered by CO poison as a function of temperature for 2% CO/H_2 and 30% CO/H_2.

where K is the equilibrium constant, p is the gas phase partial pressure and θ is the surface coverage. If K is small, the Henry's Law isotherm results so that, as an approximation:

$$\ln\theta \simeq \frac{-\Delta H}{RT} + C \qquad \text{Equation (11)}$$

where C is a constant. Because the adsorption is exothermic, $\ln\theta$ increases with reciprocal temperature. As a first approximation, then, one would expect the logarithm of the carbon monoxide coverage to change approximately linearly with temperature. This relationship is demonstrated in Figure 23.

4. SUMMARY

In this program a number of high surface area platinum on carbon supported electrocatalysts were prepared, characterized for surface area, and investigated in terms of their electrocatalytic activity. The catalysts were typically prepared at 10% Pt loading by an impregnation technique. A definite correlation was found between the specific metal surface area and the support BET surface area.

The catalysts were characterized for surface area by chemisorption, microscopic, and x-ray techniques. The surface area estimates by all techniques were comparable. Using high resolution phase contrast microscopy, the crystal lattice of highly dispersed platinum on carbon was resolved and the lattice spacing for small crystallites was measured to within 2% of the value for bulk platinum.

The oxygen reduction activity exhibited an apparent platinum crystallite size effect; however, this was thought to be caused by diffusion limitations. The apparent activation energy for oxygen reduction was estimated to be about 13 k.cal/mole, approximately one half that estimated by other researchers. The one-half relationship is known to exist for catalysts governed by diffusion factors.

It was demonstrated that the hydrogen oxidation electrode was also governed by diffusion effects; however, it was shown that the gas diffusion properties could be improved by changing the electrode structure. Activity under carbon monoxide poisoning conditions was also investigated. Isobars for 2% and 30% carbon monoxide levels in hydrogen fuel streams were measured by comparing the hydrogen oxidation current density obtained in the presence of carbon monoxide to that obtained in the absence of carbon monoxide.

REFERENCES

1. L. J. Bregoli, Electrochimica Acta, 23, 489 (1978).

2. K. Kinoshita and P. Stonehart, in "Modern Aspects of Electrochemistry, Vol. 12, Ed. J. O'M. Bockris and B. E. Conway, pp. 183-266, Plenum, New York (1977).

3. H. L. Gruber, Anal. Chem. 34, 1831 (1962).

4. H. L. Gruber, J. Phys. Chem., 66, 48 (1962).

5. S. Gilman, J. Phys. Chem. 67, 78 (1963).

6. J. Bett, K. Kinoshita, K. Routsis and P. Stonehart, J. of Catal. 29, 160 (1973).

7. K. Kinoshita, J. Lundquist and P. Stonehart, J. Cat. 31, 325 (1973).

8. E. B. Prestridge, G. H. Via and J. H. Sinfelt, J. Cat. 50, 115 (1977).

9. L. L. Ban and W. M. Hess, in "Petroleum Derived Carbons," M. L. Deviney and T. M. O'Grady eds., pp. 358-377, American Chemical Society, Washington, D.C. (1976).

10. Norelco Reporter, 16 (1), 1 (1969).

11. JEOL News, 16E (2), 20 (1978).

12. K. Kordesch, "Survey About Carbon and Its Role in Phosphoric Acid Fuel Cells," (1979).

13. "Catalyst Sintering Studies," EPRI Project 853-1 Interim Report EPRI EM-661, pp. 3-6 (March 1978).

14. M. M. Dubinin, in "Surface Area Determination," Ed. D. H. Everett and R. H. Ottewill, p. 123, Butterworths, London (1970).

15. J. Giner and S. Smith, Electrochemical Technology, 5, 59 (1967).

16. K. Kordesch and A. Marko, J. Electrochem. Soc., 107, 480 (1960).

17. "Electrode Optimization for Phosphoric Acid Fuel Cells" Technical Progress Report No. 6, DOE Contract No. ET-78-C-03-1873 Energy Research Corp. (1979).

18. H. R. Kunz and G. A. Gruver, J. Electrochem. Soc., 122, 1279, (1975).

19. W. Vogel and J. Lundquist, JECS, 117, 1512 (1970).

20. D. I. MacDonald and J. R. Boyack, J. Chem. Eng. Data, 14, 380 (1969).

21. J. Appleby, J. Electroanal. Chem., 24, 97 (1970).

22. E. Q. Thiele, Ind. Eng. Chem., 31, 916 (1939).

REFERENCES

23. P. Stonehart and P. N. Ross, Cat. Rev., 12, 1 (1975).

24. D. Ferrier, K. Kinoshita, J. McHardy, and P. Stonehart, Electroanalytical Chem. and Interfacial Electrochemistry, 61, 233 (1975).